Novel Minor Groove Binders cure animal African trypanosomiasis in an *in vivo* mouse model

Federica Giordani[1,2], Abedawn I. Khalaf[3], Kirsten Gillingwater[4,5], Jane C. Munday[1], Harry P. de Koning[2], Colin J. Suckling[3], Michael P. Barrett[1,2,6] and Fraser J. Scott[7]*

[1]Wellcome Trust Centre for Molecular Parasitology, Institute of Infection, Immunity and Inflammation, College of Medical, Veterinary and Life Sciences, University of Glasgow, Glasgow, UK, G12 8TA

[2]Institute of Infection, Immunity and Inflammation, College of Medical, Veterinary and Life Sciences, University of Glasgow, Glasgow, UK, G12 8TA

[3]Department of Pure and Applied Chemistry, WestCHEM, University of Strathclyde, Glasgow, UK, G1 1XL

[4]Parasite Chemotherapy, Department of Medical Parasitology and Infection Biology, Swiss Tropical and Public Health Institute, Basel, Switzerland, 4051

[5]University of Basel, Basel, Switzerland, 4001

[6]Glasgow Polyomics, University of Glasgow, Glasgow, UK, G61 1QH

[7]Department of Biological and Geographical Sciences, School of Applied Sciences, University of Huddersfield, Huddersfield, UK, HD1 3DH

Abstract

Animal African trypanosomiasis (AAT) is a significant socioeconomic burden for sub-Saharan Africa due to its huge impact on livestock health. Existing therapies including those based upon Minor Groove Binders (MGBs), such as the diamidines, which have been used for decades, have now lost efficacy in some places due to the emergence of resistant parasites. Consequently, the need for new

chemotherapies is urgent. Here, we describe a structurally distinct class of MGBs, Strathclyde MGBs (S-MGBs), which display excellent *in vitro* activities against the principal causative organisms of AAT, *Trypanosoma congolense* and *T. vivax*. We also show the cure of *T. congolense*-infected mice by a number of these compounds. In particular, we identify **S-MGB-234**, compound **7**, as curative using 2 applications of 50 mg/kg intraperitoneally. Crucially, we demonstrate that S-MGBs do not show cross-resistance with the current diamidine drugs and are not internalised via the transporters used by diamidines. This study demonstrates that S-MGBs have significant potential as novel therapeutic agents for animal African trypanosomiasis.

Introduction

African animal trypanosomiasis (AAT), or nagana, is a major obstacle to livestock production and, therefore, to the development of rural areas of sub-Saharan Africa. AAT is a complex of diseases mainly caused by three tsetse-transmissible trypanosome species: *Trypanosoma congolense*, *T. vivax* and, to a lesser extent, *T. brucei* spp. Although all domesticated animals can be infected by trypanosomes, cattle are the main economically and clinically relevant host (1). Most AAT cases are chronic, with animals presenting with anaemia, weight loss, weakness, immunosuppression, sterility and decrease in milk production. Death of susceptible animals is a common outcome. Thus, AAT significantly limits agricultural development and food production and, consequently, socioeconomic growth. It is a considerable cause of poverty in African rural communities, with total losses estimated at US$ 4.75 billion per year (2).

Control of AAT relies heavily on chemotherapy or chemoprophylaxis (3). Only two compounds are widely used, irrespective of the infecting species (Fig. 1): diminazene diaceturate, **1**, a diamidine and DNA minor groove binder used for cure, and isometamidium chloride, **2**, a hybrid molecule of ethidium and diminazene used for both cure and prophylaxis. In addition, the DNA intercalator ethidium bromide, **3**, is available for treatment and also gives some short-term prophylaxis (3). All these compounds have toxic effects on animals and their efficacy is undermined by increasing drug resistance (4-8). Despite the high usage levels (at least 35 million doses/year), pharmaceutical companies are disengaged from this area due to the lack of commercial incentive. Consequently, since the introduction of diminazene and isometamidium more than 50 years ago, no progress has been made towards new AAT chemotherapy. However, a renewed interest in alternative veterinary trypanocides has emerged due to the disease's impact on food security, and the engagement of a Product Development partnership, the Global Alliance for Livestock Veterinary Medicines (GALVmed), has provided new coordination in tackling the problem.

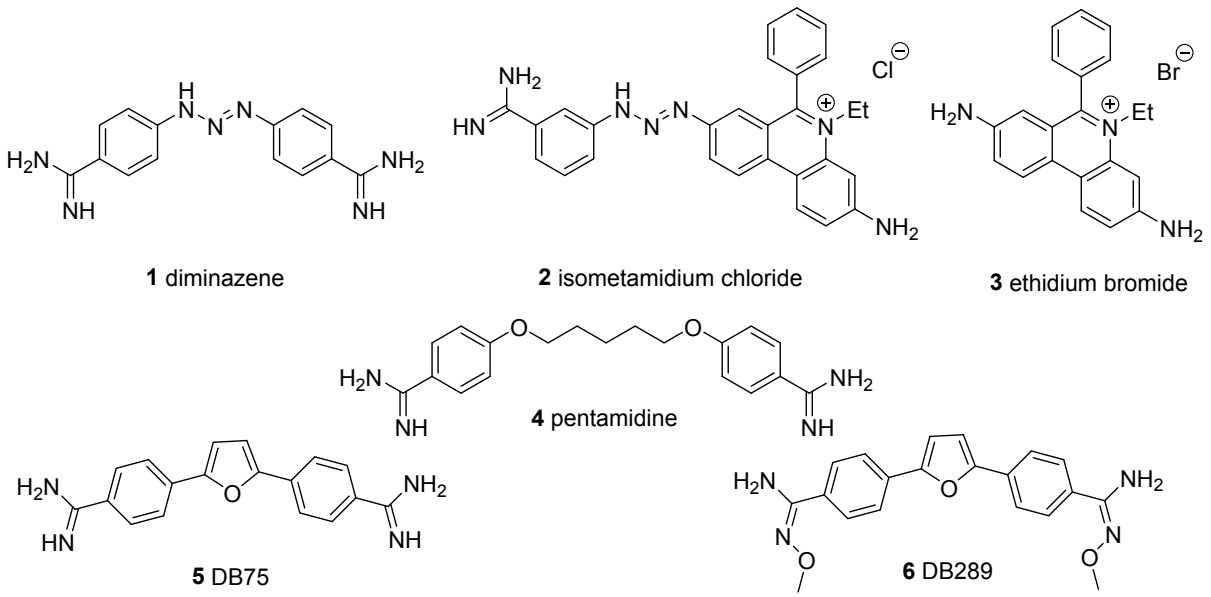

Figure 1. Chemical structures of the three main compounds used for treatment and prophylaxis of AAT and of the arylamidines pentamidine, DB75 and DB289.

Minor groove binders (MGBs) comprise several classes of compounds that bind to the minor groove of DNA and have been used as therapies for both human and animal infections (9-11). Diminazene, **1**, is an example of the diamidine class of MGBs, which also includes pentamidine, **4**, (Fig. 1), a compound with a broad antimicrobial activity (11). Pentamidine has been used most notably as a treatment for human African trypanosomiasis (HAT); however, it suffers from toxicity issues and poor oral availability, requiring parenteral administration for systemic infections (11). The di-arylamidines were used as the basis of a synthesis campaign by Boykin and co-workers, which led to the discovery of DB75, **5**, (furamidine, Fig. 1), a highly active antitrypanosomal drug in animal studies, and its orally available prodrug DB289, **6**, (pafuramidine, Fig. 1) (12, 13). Pafuramidine, **6**, concluded Phase II/III clinical trials against early-stage HAT before renal toxicity in a retrospective phase I safety trial led to its development being discontinued (14). Yet, this trial once again underscored the clinical efficacy of MGBs (with the toxicity attributable to the pro-drug strategy (14), and the enormous impact of diminazene and pentamidine as the most essential trypanocides to date serves as a reminder of the potential of MGBs as antiparasitic therapies (11). Crucially, cross-

resistance with existing diamidine drugs does not occur if the diamidine transport mechanisms are avoided (15).

Strathclyde minor groove binders (S-MGBs) are a distinct family of DNA-binding compounds derived from the structure of the natural product distamycin (16). S-MGBs include a diverse array of structural features allowing for extensive coverage of structural and property space within the same DNA-binding template (17). The main sites where variation is introduced in S-MGBs are the head groups and the specific linker moiety used to connect to the rest of the molecule (amidine, amide or alkene), the particular heterocycle, the alkyl substituents on the heterocycle, and the basicity of the C-terminal tail group (18). Through altering these structural features, potent antibacterial compounds have been discovered, one of which, MGB-BP-3, is about to enter a Phase IIa clinical trial against *Clostridium difficile* infections (19). A variety of MGB-BP-3 analogues have been shown to be active against *T. brucei* and *Plasmodium falciparum* (20, 21), both in cell-based studies and in *in vivo* disease models, and against *Leishmania major* and *L. donovani* in culture (unpublished results). A potential benefit of targeting DNA is that it is to be expected that many binding sites will be occupied by S-MGBs, leading to complex cellular perturbations, which could mitigate the risk of rapidly developing resistance. Conversely, the ubiquity of DNA makes species selectivity critical and this has been a challenge for some previous generations of MGBs. In the context of S-MGBs, selectivity can be obtained between different infectious organisms and mammalian cells giving rise to therapeutic ratios indicative of selective drug candidates (16 - 19, 22).

In this paper we describe the activity of S-MGBs against the animal infective parasites *T. congolense* and *T. vivax*, from which an initial SAR was developed. Three S-MGBs were advanced to *in vivo* proof of concept evaluation in a mouse model of *T. congolense* infection. Two of these were curative and, crucially, displayed no cross-resistance with currently used trypanocides. Furthermore, we present the results of an initial investigation into the mechanism of action of the lead compound, **S-MGB-234**, **7**.

Results

Structure-activity relationship revealed. A substantial and representative collection of S-MGBs was screened for activity against *T. congolense* and *T. vivax*, and in parallel against L6 rat myoblast cells as an indicator for mammalian cell toxicity. S-MGBs were selected in order for the collection to explore a large chemical space from our entire S-MGB library. Those compounds of interest to SAR discussions are presented in Table 1 (full data set in Table S1). Most of the compounds studied have been previously described (16, 17, 18, 21), but several are novel. Details of the synthesis of novel compounds from Table 1 are outlined in Scheme 1 below. Briefly, the appropriate nitro pyrrole dimer was converted to the corresponding amine by reduction with hydrogen gas over palladium on carbon. This amine was then coupled to the appropriate carboxylic acid using HBTU to form the final S-MGB. Syntheses of the specific nitro pyrrole dimers and carboxylic acids have been previously reported, and are referenced in the experimental section.

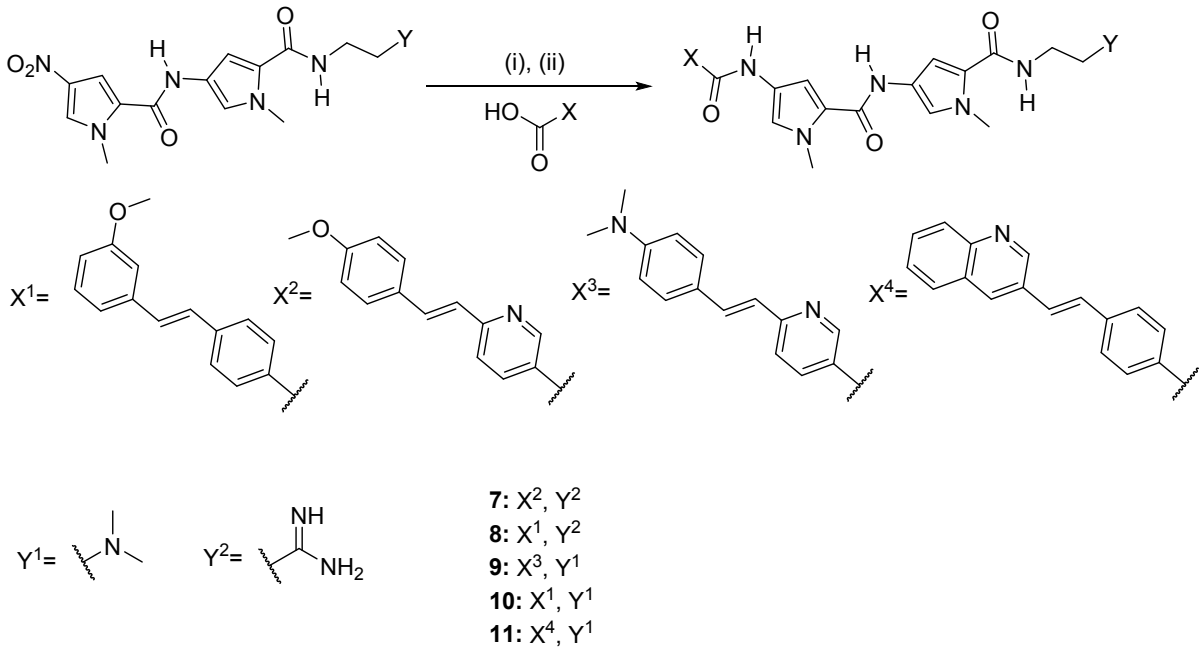

Scheme 1. Synthesis of novel MGBs from Table 1. (i) H_2, Pd/C, MeOH, not isolated (ii) Carboxylic acid, HBTU, DMF.

The full data set presented in Table S1 identify several structural features that appear to improve activity against *T. congolense* and/or *T. vivax*. The following discussion summarises the principal observations, with Table 1 summarising the activities and structures of the compounds of interest, but Table S1 should be referred to for the full data set.

Table 1. Activity of a collection of S-MGBs against *T. congolense*, *T. vivax* and L6 cells

		EC_{50} (μM)			SI	
Compound	S-MGB Structure	*T. congolense* IL3000	*T. vivax* STIB 719	L6	L6/*T. congolense*	L6/*T. vivax*
7	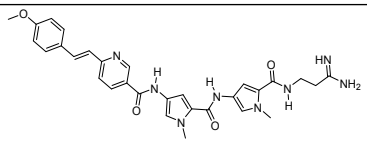	0.09±0.01	0.45±0.24	20.39±3.3	232.8	45.0
8	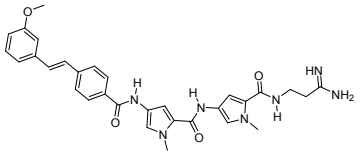	0.08±0.00	1.15±0.65	28.56±3.57	343.8	24.8
9	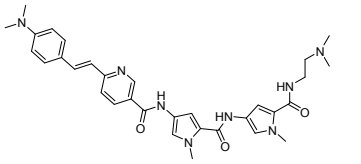	0.79±0.05	0.15±0.08	1.98±0.19	2.5	13.6
10	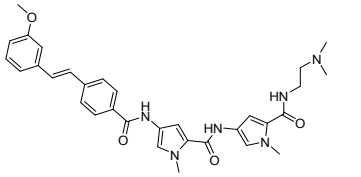	1.27±0.43	0.54±0.29	8.86±3.46	7.0	16.6
11	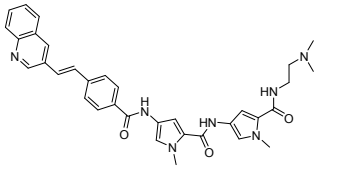	0.07±0.01	0.13±0.02	4.23±1.41	61.8	33.4

12[17]	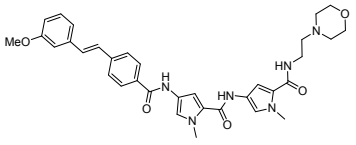	1.85±0.58	1.27±0.05	20.22±2.18	10.9	15.9
13[17]	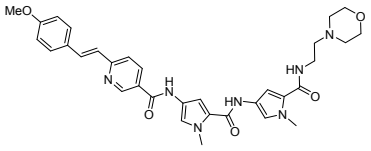	2.96±1.19	1.67±0.06	3.76±2.18	1.3	2.3
14[20]	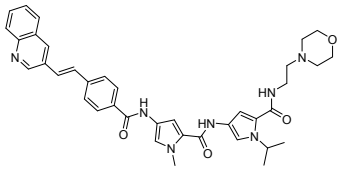	0.18±0.06	0.01±0.00	0.26±0.02	1.4	26
15[20]	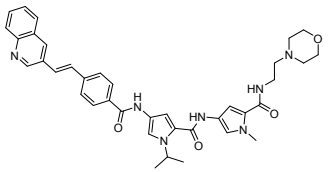	0.06±0.02	0.02±0.01	0.04±0.01	0.7	1.9

Data are reported as a mean of 3 experiments ± standard deviation, reported to two decimal places; SI, selectivity index calculated by division of the indicated mean values, reported to one decimal place.

Several compounds displayed EC_{50} values against *T. congolense* below 100 nM (**15**, **8**, **7**) and two of these contained the 3-quinolylalkenyl head group. Against *T. vivax,* compounds active at 100 nM or less also contained the 3-quinolylalkenyl head group (**14**, **15**, **11**). Indeed, alkenyl head groups, especially those containing the 3-quinolyl group, led to the strongest activity against both species; other aryl alkenes and related fused heterocyclic alkenes were in general much more weakly active. Although some 3-quinolyl alkenes were toxic to rat L6 cells, the selectivity index (SI) of one of these (**11**) was >30 fold. The structure of the tail group also affected the differential activity. Both the amidinylethyl and dimethylaminoethyl/propyl series included active compounds with very good SI values, especially relative to *T. congolense* (**7**, **8, 11**). Further, as shown by the L6 cell-based assay, the effect of a number of substructures on cytotoxicity could be identified. Compounds that contained amidine-linked head groups, trifluoromethylphenyl, or benzoxazole head groups, or long side chains were predominantly inactive In general, compounds containing amide-linked head groups were poorly active as well as non-toxic to L6 cells (Table S1). However, bearing in mind the variations in

trypanocidal activity of amidine- and alkene-containing head groups, it may simply be that active amide head groups have not yet been identified. On the basis of their intrinsic antitrypanosomal activity and favourable SIs, a small subset of S-MGBs (**7**, **8** and **11)** was selected for further *in vitro* evaluation, along with some additional compounds for comparison purposes (**12**, **13**, **9** and **10**).

Absence of cross-resistance to diamidines. As noted above, the diamidine class of MGBs, which has been in use for over 60 years against trypanosomiasis, has suffered from the emergence of resistance by the parasites (23 - 25). It was important, therefore, to establish whether the S-MGBs here identified as trypanotoxic retained activity in diamidine-resistant trypanosomes. To assess this, a small subset of S-MGBs from the initial screen, including the most therapeutically relevant, was tested against two diminazene-resistant *T. congolense* lines generated *in vitro*. Our results revealed no decrease in activity of the S-MGBs against the diminazene-resistant lines, which instead showed a modest but significant hypersensitivity to some of the compounds (Fig. 2a and Table S2 for all data).

In *T. brucei,* resistance to diamidines including diminazene and furamidine is linked to loss of activity of specific plasma membrane transporters *Tb*AT1/P2 (26-28) and, in the case of pentamidine, also of HAPT/AQP2 (29, 30), that mediate their uptake into this parasite. *Tb*AT1/P2 impairment also causes cross-resistance to compounds which contain the same *Tb*AT1/P2 recognition motifs, including the melaminophenyl arsenicals melarsoprol and cymelarsan (26, 31). In order to determine the potential for cross-resistance developing as a result of sharing the same route of cellular entry, the S-MGBs were evaluated as substrates for these known MGB transporters. The same subset of compounds listed above was tested against *T. b. brucei* lines lacking only *Tb*AT1/P2 (*tbat1*$^{-/-}$ line (26)) or both *Tb*AT1/P2 and HAPT/AQP2 (B48 line (29). The experiments showed that trypanosomes not expressing these drug transporters, and therefore resistant to diminazene, generally retained sensitivity to the S-MGBs (Fig. 2b and Table S3 for all data), with only a minor increase in EC_{50} (1.5 fold) for **9** against the *tbat1*$^{-/-}$ and B48 lines and for **7** against the B48 line. These data confirmed that the activity of S-MGBs is not (principally) dependent on the expression of *T. brucei Tb*AT1/P2 or HAPT/AQP2 and that the S-MGBs are not cross-resistant with current diamidines. This is an important further

indication of the differences between S-MGBs and other classes of MGBs such as the diamidines. Of note, *T. congolense* lacks a functional equivalent of *Tb*AT1/P2 (32), and HAPT/AQP2 (unpublished data), although other *T. brucei* group trypanosomes (incl. *T. equiperdum*, *T. evansi*, *T. b. gambiense*, *T. b. rhodesiense* (33-36)) most likely do. We conclude that diamidines and S-MGBs must enter via other, as yet unidentified, routes in *T. congolense* and, based on the absence of cross-resistance (Figure 2 and Tables S2 and S3), that S-MGBs do not share uptake routes with diamidines in either *T. brucei* or *T. congolense.*

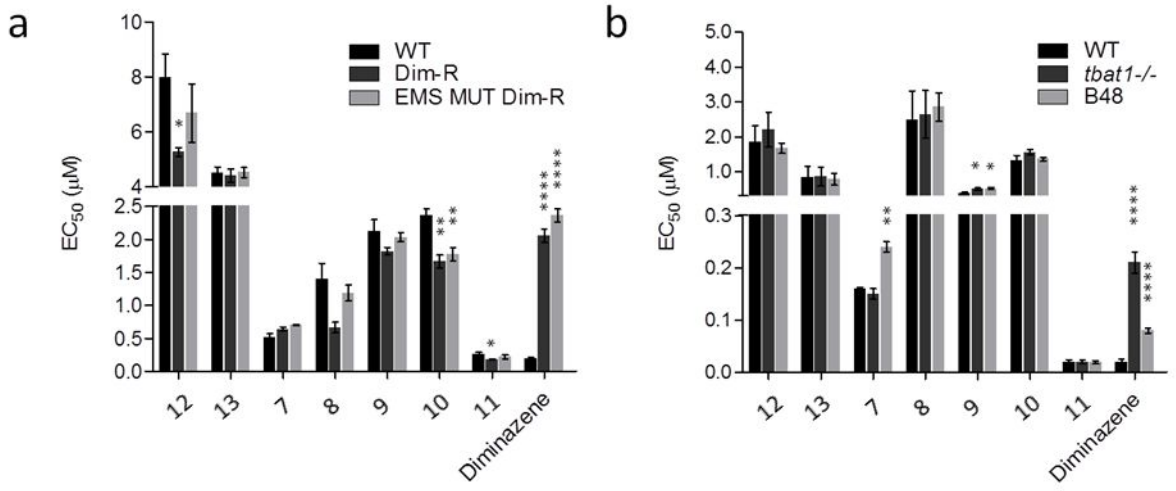

Figure 2. S-MGBs retain trypanocidal activity *in vitro* against diminazene-resistant *T. congolense* and *T. b. brucei* lines. **a** *T. congolense* diminazene-resistant lines DimR and EMS MUT DimR. The EC_{50} values against *T. congolense* presented in this figure were obtained using a different protocol from that of the initial compound screen (data in Table 1 and Table S1), hence the difference in absolute values between the two datasets. **b** *T. b. brucei tbat1*$^{-/-}$ lacks the P2 amino-purine transporter *Tb*AT1/P2 (26) and line B48 lacks both *Tb*AT1 and HAPT/AQP2 activity (29). (Mean ± SEM, n≥3). Statistical significance to untreated wild type (WT) line was assessed by unpaired *t*-test: * $p<0.05$; ** $p<0.01$; **** $p<0.0001$.

***In vivo* efficacy of S-MGBs in an experimental model of *T. congolense* infection.** Compounds **7**, **8** and **11** were further progressed for *in vivo* efficacy studies in a mouse model of infection with *T. congolense* STIB 736/IL1180. Mice were infected intraperitoneally (i.p.) with *T. congolense* and parasitaemia was allowed to develop before treatment with the three selected compounds. At the end of a 2-month monitoring period, aparasitaemic mice were considered cured (37). The therapeutic effect of each compound is shown in Table 2.

Table 2. *In vivo* efficacy of selected S-MGBs in the *T. congolense* (STIB 736/IL1180) experimental mouse model of infection.

S-MGB-ID	Dose (mg/kg/day × number of treatment days)	Cured/ infected	MRD (days)	MSD (days)
7[a]	50 × 4	toxic	n/a	n/a
	50 × 2	4/4	n/a	>60
	10 × 4	1/4	19.3	34.75
	10 × 2	0/4	12.5	19.5
8[a]	50 × 4	toxic	n/a	n/a
	50 × 2	toxic	n/a	n/a
	10 × 4	4/4	n/a	>60
	10 × 2	4/4	n/a	>60
	10 × 1	3/4	7	>51
	5 × 2	3/4	4	>50.25
11[a]	50 × 4	toxic	n/a	n/a
	50 × 2	1/4	11	>29.25
	10 × 4	0/4	5.5	15

	10 × 2	0/4	4	11
Untreated	n/a	0/4	n/a	11

[a] Vehicle 10% DMSO in water solution; MRD, mean day of relapse; MSD, mean day of survival; n/a, not applicable.

7 provided total cure and no relapses in mice (4/4), when treated with 2 applications of 50 mg/kg i.p. Partial cure (1/4) was seen in mice treated with 4 daily applications of 10 mg/kg i.p., whilst only 2 applications of **7** at 10 mg/kg i.p. gave no cure but prolonged survival relative to the untreated control. **8** was fully curative (4/4) when administered as either 4 or 2 applications at the lower dose of 10 mg/kg i.p. At a total dose of 10 mg/kg, given as a single treatment i.p., or as 2 applications of 5 mg/kg i.p. 24 hours apart, a similar curative efficacy (3/4) was seen for both administrative regimens.

Only a partial cure (1/4) was achieved with **11** in mice treated with 2 applications of 50 mg/kg i.p., with average relapse and survival days of 11 and >29.25, respectively. No cure was seen at 10 mg/kg i.p., at either 2 or 4 daily administrations, with marginal effects on survival. Full cure with **11**, e. g. at 50 × 4 mg/kg was attempted but could not be achieved due to apparent toxicity at the higher dosages.

These data show efficacious treatment of a *T. congolense* mouse model of infection for two out of three S-MGBs at non-toxic dosage regimens. Although **8** performed slightly better in the *T. congolense* mouse model of infection, **7** was selected as our lead compound for further investigative studies due to its higher activity in the *in vitro T. vivax* assay, together with two fluorescent S-MGBs with less activity.

Intracellular distribution into trypanosomes. The intrinsic fluorescence of some S-MGBs makes it possible to investigate their intracellular distribution in trypanosomes following incubation. As previously shown for *T. b. brucei* (21), experiments with the highly fluorescent **9** confirmed internalisation in *T. congolense* (Fig. 3a). The main visible cellular targets, clearly detectable using the FITC filter, were the nucleic acids (nucleus and kinetoplast), as expected for these MGBs, many of which have been shown to bind strongly to AT sites of DNA by footprinting and biophysical

methods (22). DAPI colocalisation with both **9** and another fluorescent S-MGB, **16**, confirmed organelle identification, and showed that DAPI staining of the kinetoplast abolished S-MGBs fluorescence in this organelle (Fig. S1). Despite thorough washing of *T. brucei* labelled with **16** and **9**, the fluorophores were retained in both DNA-containing organelles (data not shown). Together with the main fluorescent emission observed under the green channel, **9** (and the other fluorescent S-MGBs) also emitted at longer wavelength, labelling other subcellular structures visible under DsRed filter. In particular, a bright vesicle posterior to the nucleus was clearly visible under the DsRed filter. The accumulation of S-MGBs in organelles other than the nucleus and kinetoplast adds complications to the understanding of their mechanism of action. Binding to the DNA double helix or interference with DNA-protein interactions are obvious targets for S-MGBs but there may be others as yet unidentified.

Metabolomics analysis. An untargeted metabolomics analysis was performed using **7** to assess the effects of S-MGBs on the metabolism of *T. b. brucei* (Fig. 3b). Results showed an accumulation of 15 putatively identified metabolites (p <0.05, >2 fold change) in treated parasites (Fig. 3b and Table S4), with a preponderance of metabolites involved in nucleotide metabolism, particularly pyrimidine metabolism. Among these, the pyrimidine nucleoside deoxyuridine showed the largest increase (> 7 fold compared to DMSO control), followed by other pyrimidines: cytosine, cytidine, dCTP, uridine, dUMP, dAMP and dihydrouridine. The accumulation of the purine derivative hypoxanthine was also recorded.

Among the other putative metabolites emerging from the analysis, creatinine is believed to be irrelevant to trypanosome metabolism and probably accumulated from serum present in the medium. The observed changes in levels of various cofactors (including pyridoxine, pyridoxamine, dethiobiotin) are intriguing, but so far their significance remains elusive.

Taken together, the metabolomics data seems to indicate that the S-MGBs interfere with the integrity and /or functions of nucleic acids, with the most notable perturbations in nucleotide metabolism, while most of the metabolome remained unaffected following 8 hours of treatment,.

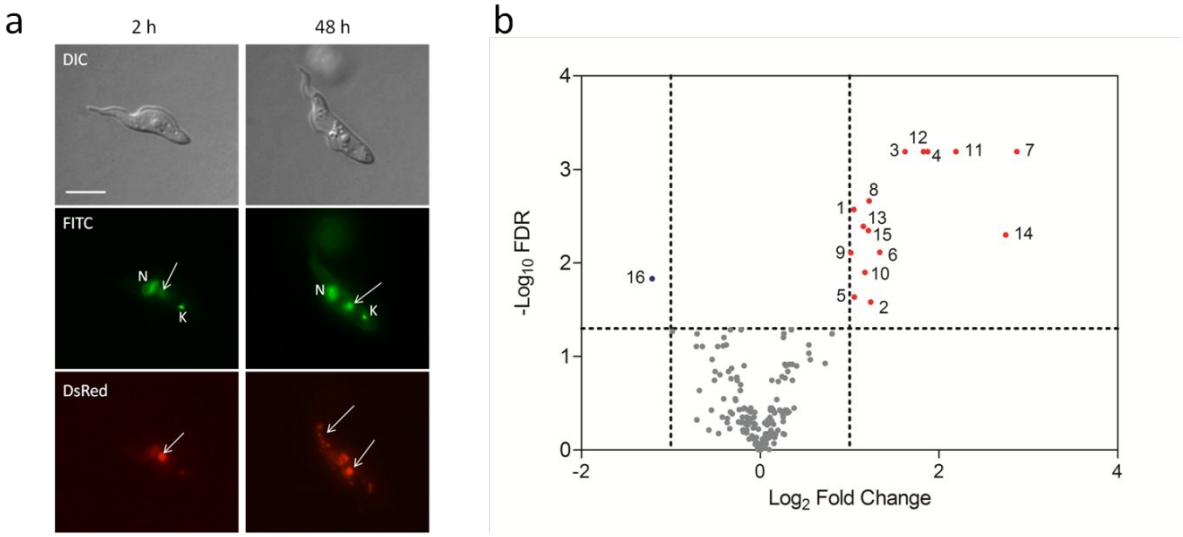

Figure 3. S-MGBs target the nucleic acids in trypanosomes. **a** Accumulation and intracellular distribution of highly fluorescent **9** (incubation with 2 × EC_{50} for 2 h or 48 h) in *T. congolense*. N, nucleus; K, kinetoplast; arrow = other stained subcellular structures. Bar = 10 μm. **b** Volcano plot of metabolic changes in *T. b. brucei* following treatment with **7** (5×EC_{50}, 8 hours). The time point was chosen based on **7** growth inhibition curve (Fig. 5a), allowing time for metabolic perturbations to emerge but avoiding cidal effects on cells. Red dots indicate putative metabolites significantly up-regulated as compared to untreated DMSO control; blue dots indicate metabolites significantly down-regulated as compared to control. Differentially abundant metabolites were identified by p <0.05 (*t*-test) statistical significance and 2 fold-change cut-off. 1) 5-6-Dihydrouridine; 2) Creatinine; 3) Cytidine; 4) Cytosine; 5) dAMP; 6) dCTP; 7) Deoxyuridine; 8) Dethiobiotin; 9) L-Lysine; 10) dUMP; 11) Hypoxanthine; 12) N6-Acetyl-L-lysine; 13) NG,NG-Dimethyl-L-arginine; 14) Pyridoxine; 15) Uridine; 16) Pyridoxamine.

Mitochondrial DNA is not the main S-MGB target. The kinetoplast (trypanosome mitochondrial DNA) has long being considered as the main subcellular target of diamidines, phenanthridines and other cationic MGBs and intercalators. Upon binding to AT-rich sites in the minor groove, diamidines cause inhibition of replication of the kDNA and its disintegration, with consequent cell death (11). Trypanosomes can adapt to survive without a (complete) mitochondrial genome, as do *T. evansi* and

T. equiperdum, but it was found that the viability of such cells depends on a compensating mutation in a nuclear-encoded F_1F_o ATPase subunit, which allows mitochondrial membrane potential to be maintained (38). These akinetoplastic parasites are less sensitive to diamidines than trypanosomes depending on an intact kinetoplast and are also more resistant to the phenanthridine class of drugs, which also target nucleic acids (39, 40). To assess whether the presence of a functional kinetoplast was equally important for the action of our S-MGBs, **7** was tested against a *T. b. brucei* line (ISMR1) where the kinetoplast has been lost following *in vitro* selection for resistance to the phenanthridine isometamidium chloride (39). **7** was equally active against the akinetoplastic line ISMR1 and the wild type line that possesses a normal kinetoplast (Fig. 4, Table S5). These results were confirmed by tests on a kinetoplast-independent *T. b. brucei* line engineered to express an F_1 ATPase γ–subunit with mutation L262P (40), which rapidly loses its normal kinetoplast under kinetoplast-targeting drug pressure because it is no longer dependent on it (Table S5). **7** activity was comparable across all these lines, suggesting that its trypanocidal activity is independent from the presence of a functional kinetoplast. These data are in sharp contrast to those obtained for the diamidine diminazene and the phenanthridines isometamidium and ethidium, to which the akinetoplastic cell lines are highly resistant (39, 40). Importantly, these data seem to preclude the emergence of cross-resistance between S-MGBs and the phenanthridine trypanocides (isometamidium chloride and ethidium bromide) currently used against AAT as the sole alternatives to diminazene aceturate.

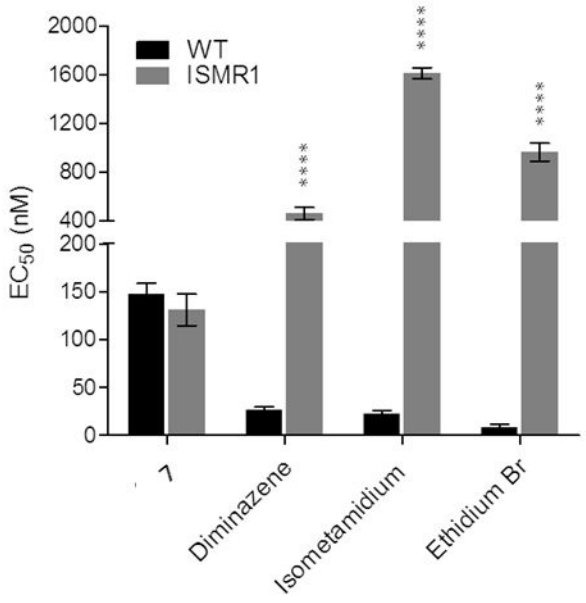

Figure 4. The kinetoplast is not required for S-MGBs trypanocidal activity. The EC_{50} value of **7** did not significantly change when the compound was tested against *T. b. brucei* ISMR1, an akinetoplastic line selected *in vitro* for resistance to isometamidium and highly cross-resistant to ethidium bromide and to diminazene.

S-MGBs affect trypanosome growth and cell cycle progression. Continuous exposure to **7** resulted in cell growth arrest of *T. b. brucei* cultures within 48 h when incubated with concentrations ≥1 × EC_{50} (i.e. 0.16 μM), with complete clearance at 10 × EC_{50} (Fig. 5a, left). Similarly, 5 × EC_{50} of **7** (2.55 μM), sterilised *T. congolense* cultures within 72 h, or after 96 h at 2 × EC_{50} (Fig. 5a right). Wash-out experiments showed that **7** has irreversible effects on trypanosome survival, indicating that this compound is cytocidal and not cytostatic (Table S6). Treated *T. congolense* were committed to death after 10 – 24 h of incubation with **7** at 5 × EC_{50}. In order to produce irreversible effects on *T. brucei* survival, higher concentrations of the compounds had to be used: exposure to 10 × EC_{50} for 10 h committed all parasites to death, possibly reflecting the need for a higher concentration gradient to achieve a lethal concentration at the intracellular site of action within this time frame. These kinetics and concentrations were comparable to those obtained for the slow acting veterinary drug diminazene (Table S6).

An analysis of the cell cycle progression of trypanosomes exposed to **7** was performed by monitoring the replication and segregation of the nuclear (N) and kinetoplast (K) genomes, which in these parasites occur in sequential, tightly regulated phases (41). This process is similar in *T. brucei* and *T. congolense*, but for our analysis we used only the former due to the tendency of *T. congolense* to clump together *in vitro*, making it difficult to distinguish individual cells.

DNA analysis of asynchronous *T. b. brucei* populations treated with **7** revealed a profound effect of the compound on normal cell cycle progression (Fig. 5b). **7** caused an accumulation of parasites with multiple kinetoplasts and nuclei (MKMN cells), seemingly cells that have started a new cell cycle without having undergone cytokinesis. At 48 h of treatment with 2 × EC_{50}, the MKMN trypanosomes constituted more than half of the cell population (Fig. 5b), but the effect was already evident when using 1 × EC_{50} (Fig. S2). The phenotype of these abnormal parasites appeared heterogeneous: along with 3K1N and 1K3N cells, trypanosomes with a much higher number of either K or N, or both, were observed.

This experiment implies that, at least for a period, the S phase is not inhibited by S-MGBs and that, while exposed to **7**, trypanosomes maintain their ability to synthesise new DNA. This was confirmed by an EdU assay, which allows monitoring of DNA synthesis by visualising the incorporation of the thymidine analogue 5-ethynyl-2′-deoxyuridine (EdU) into newly formed DNA (Fig. S3). Although a dose-dependent inhibition of DNA synthesis in *T. b. brucei* treated with **7** was observed within 8 h of incubation, this occurred only when using high concentrations of the compound (5 × EC_{50} and 10 × EC_{50}) and the inhibition was much less pronounced than that caused by the eukaryotic nuclear DNA polymerase inhibitor aphidicolin (42) (26% and 40% inhibition for 5 × EC_{50} and 10 × EC_{50}, respectively, versus 90% with aphidicolin) (Fig. S3).

It thus appears that during the first 12-24 hours of incubation at least, DNA synthesis continues, but cytokinesis is progressively affected, leading to apparent growth arrest; after this, further DNA synthesis may also be affected (cell cycle arrest), as the percentage of 1N1K cells remains largely unchanged between 24 and 48 h. The period leading into this seems to correspond to the incubation time before the cells are irreversibly committed to death, i.e. the cell cycle arrest is the point where the damage becomes irreversible.

S-MGBs-treated trypanosomes present with an abnormal phenotype. *T. b. brucei* parasites from the experiment described above often presented with nuclei abnormal in morphology, position and integrity and, in extreme cases, completely fragmented (Fig. 5c). The increase in the number of nuclei/nuclear fragments and kinetoplasts was accompanied by an increase in cell size and in the number of flagella, features typical of a block preventing cytokinesis (43).

Transmission electron micrographs of **7**-treated *T. b. brucei* parasites showed a number of cellular aberrations at 8 h of exposure, before the appearance of the conspicuous abnormal phenotype observed by light and fluorescence microscopy at longer time points. TEM revealed treated parasites with irregular, elongated nuclei (Fig. 5d panel I), and some with abnormal flagella lacking a paraflagellar rod (Fig. 5d panel II). Others revealed unusual cytoplasmic axonemes, enlarged rough endoplasmic reticulum (Fig. 5d panel III) and an increase in multi-vesicular bodies (Fig. 5d panel II) when compared to DMSO-treated control parasites. These results suggest that, upon treatment with **7**, trypanosomes encounter problems with cytokinesis, mitosis and flagellar pocket biogenesis, consistent with the subsequent cell cycle defects observed, in particular the accumulation of multi-nucleated and multi-flagellated cells.

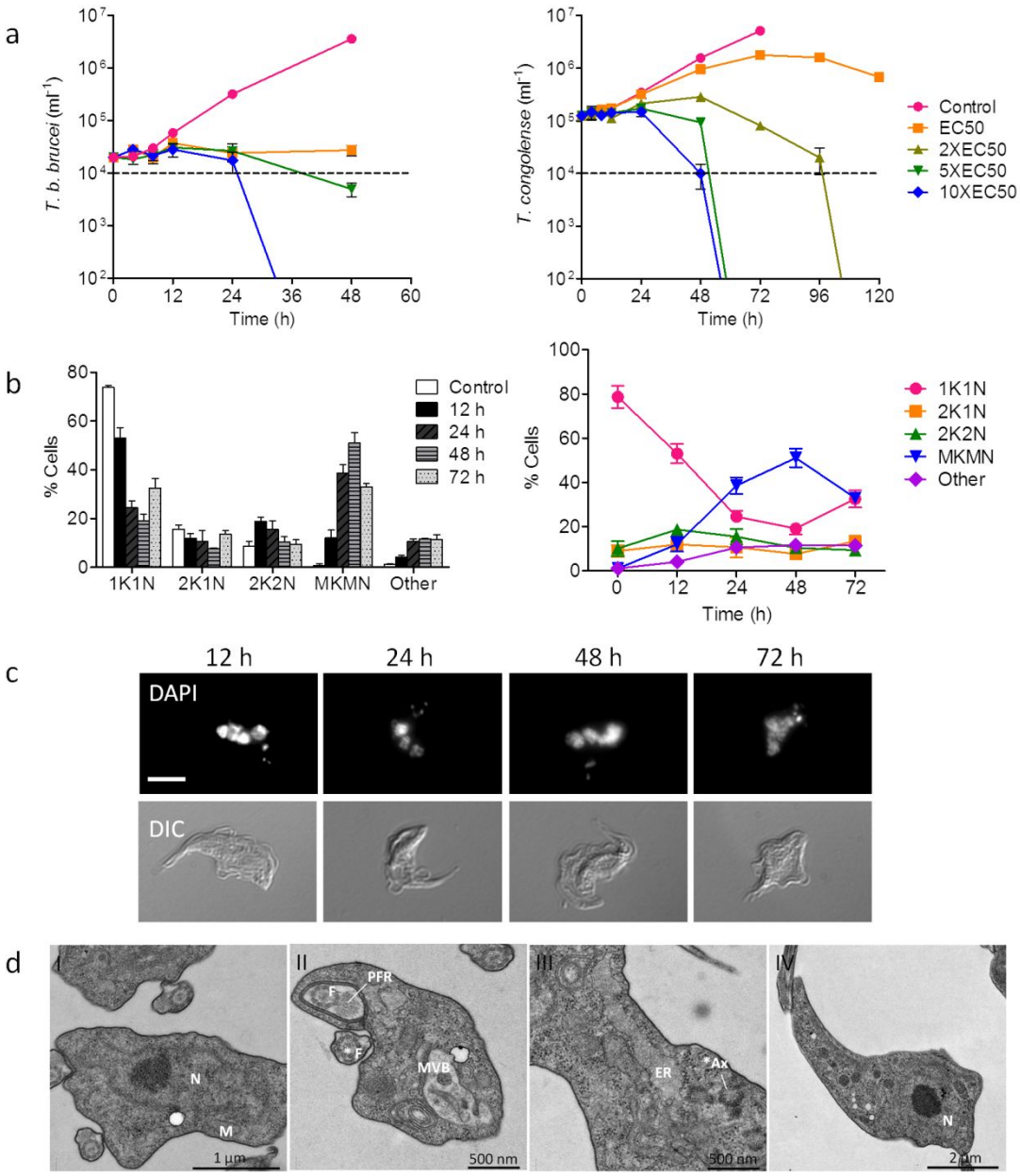

Figure 5. S-MGBs affect cell division and cell cycle progression. **a** Growth inhibition curves of cultures of *T. b. brucei* (left) and *T. congolense* (right) continuously exposed to different doses of **7** (mean ± SEM, n≥3). **b** Left: quantification of the proportion of different cell types (based on the nucleus -N- and kinetoplast -K- configuration) of *T. b. brucei* exposed to **7** (2 × EC_{50}). Cells with 1K1N are in G1 or S phase; the kinetoplast S phase starts before nuclear S phase and is shorter than the latter, resulting in 2K1N cells in G2/M phase; the nucleus then divides during mitosis, generating 2K2N post-mitotic cells, which undergo cytokinesis. The values for the untreated sample refer to the 12 h time point. Right: quantification of the proportion of different cell types over time; more than

200 cells were analysed per sample (mean ± SEM, n=3). **c** DAPI-stained and corresponding DIC images of treated *T. b. brucei* (2 × EC_{50} of **7**) from the same experiment; bar = 10 μm. **d** Representative transmission electron microscopy images of *T. b. brucei* treated with **7** (2 × EC_{50}, 8 h) **(**panels I-III**),** and with DMSO as a control (panel IV). N, nucleus; M, mitochondrion; F, flagellum; PFR, paraflagellar rod; MVB, multivesicular bodies; ER, rough endoplasmic reticulum; *F, flagellum without paraflagellar rod; *Ax, cytoplasmic axoneme. The EC_{50} values used for these experiments refer to those presented for the wild type in Table S2 and Table S3.

Discussion and Conclusion

Structure-activity relationships of anti-trypanosomal S-MGBs. Antimicrobial MGBs are generally active if they can reach target DNA and bind to it, thereby disrupting DNA function (44, 45). S-MGBs show a relative lack of activity against Gram-negative bacteria compared with Gram-positive bacteria (46) apparently because they penetrate the Gram-negative membrane poorly if at all. Access to DNA is also important in mammalian cell toxicity. With the current state of knowledge it is not yet possible to design compounds with the required species selectivity for minor groove binders and it is necessary to proceed empirically. Fortunately, each trypanosome species studied here shows a similar S-MGB SAR, probably reflecting a similar mechanism of cellular uptake, from which selective activity of MGBs commonly arises (47).

The possibility of developing a single compound with potent activity against both *T. congolense* and *T. vivax* is examined in Figure 6a, which shows a modest general correlation. The best compounds in this regard, **14** and **15,** being found towards the lower left hand corner. However, both are essentially equitoxic to L6 cells and *T. congolense* / *T. vivax*, and it is evident that selectivity must outweigh trypanocidal activity. Thus, high activity against both species together with an acceptable selectivity index to mammalian cells is required for further development of compounds beyond this initial study and Figure 6b allows all three parameters to be visualized (Figs. S4 and S5 show this data in two separate plots). From this analysis **11** is a better starting point for further development than more active compounds in their proximity in Figure 6a, based on their moderate toxicity to L6 cells. The even lower toxicities associated with the amidine-containing tail groups in compounds **7** and **8** are also clearly evident. This high pK_a tail group is a major determinant in the physicochemical properties of the S-MGBs leading to compounds protonated at physiological pH and is expected to be particularly important with respect to cellular uptake, intracellular distribution and efflux (46).

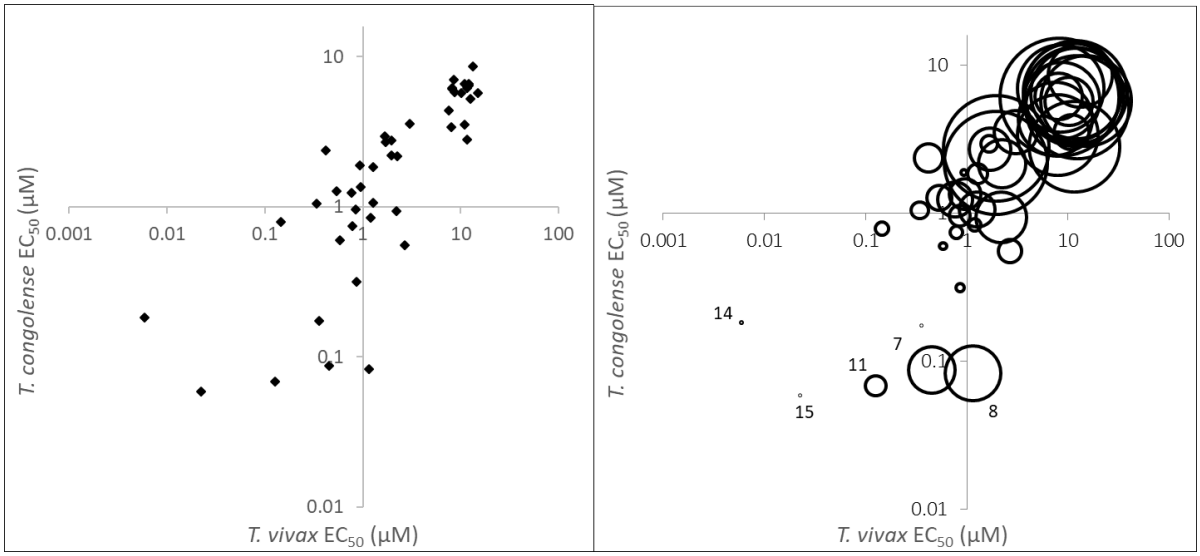

Figure 6. S-MGBs SAR revealed. **a** Comparative activities against *T. vivax* and *T. congolense.* The compounds with best activity against both trypanosome species are found towards the lower left hand corner of the plot. **b** Same data as **a**, but with additional L6 cytotoxicity represented as bubble plot – the lower the EC_{50} against L6, the smaller the bubble.

Of the three compounds evaluated *in vivo*, **11** had the poorest selectivity index (64) when comparing the activity against *T. congolense in vitro* with the cytotoxicity against L6 cells. Both **7** and **8** had selectivity indices greater than 200 and, unlike **11**, were able to elicit complete cure at non-toxic doses.

Differentiating S-MGBs from other anti-trypanosomal MGBs. Our results on diminazene-resistant *T. congolense* strains gave no indication of cross-resistance with the diamidine class of compounds, which is a factor of crucial importance for the future development of the S-MGBs as trypanocidal agents for AAT. Although both groups of molecules target the minor groove of DNA, preferences for different sequences might result in non-overlapping activities, although both are believed to preferentially bind A/T-rich sequences. A more probable explanation for this lack of cross-resistance, however, is the separate MGB classes entering trypanosomes by different routes, i.e. the S-MGBs do not enter trypanosomes via the same transporters that take up diamidines. Indeed, we observed no differences in S-MGB activity when tested on *T. b. brucei* lines lacking either *Tb*AT1/P2 or both

*Tb*AT1/P2 and HAPT/AQP2 transporters. Moreover, *T. congolense* does not have a syntenic equivalent to *Tb*AT1, and its P1-type purine nucleoside transporter *Tco*AT1, inaccurately reported as being equivalent to *Tb*AT1, does not recognise diminazene as a substrate (32). The transporters for the phenanthridines, ethidium and isometamidium have not yet been identified but their accumulation appears to be a balance between uptake and efflux across the plasma membrane with the driving force being the mitochondrial membrane potential segregating the drug in the mitochondrion (39, 48).

Distamycin A, the prototype MGB, has well-known affinity for AT-rich regions of DNA. It binds to regions with 4 or 5 AT base pairs, altering the double helix conformation and interfering with the binding of nuclear proteins (49). Derivatives of distamycin A, such as S-MGBs, are likewise expected to have a direct or indirect action on nucleic acid functions and/or replication, resulting in their trypanocidal activity. Evidence here shows that S-MGBs do indeed concentrate in the kinetoplast and nucleus. This is different from what is seen with the diamidines, which accumulate predominantly in the mitochondrion and have high affinity for the kinetoplast DNA. This explains why the absence of an intact kinetoplast is not linked to resistance to the S-MGBs, ruling it out as a main target. This does not mean S-MGBs do no damage the kinetoplast; rather, they also target the nucleus and the uncharged compound of the series will likely achieve the highest concentration initially in the cytoplasm.

Interestingly, the fluorescent S-MGBs were detected in cellular compartments other than the nucleus and kinetoplast, although it is unclear whether this might contribute to their trypanocidal activity or only represents a storage sink for the compounds. The brightly stained vesicle observed in treated *T. congolense* cells could correspond to what Vickerman defined as the "sac of secretion" (50), later called the "digestive vacuole", which is part of the endocytic apparatus of this parasite (51). Further work is needed to clarify if this is linked to the mechanism of internalisation of S-MGBs but endocytosis after binding to surface proteins could indeed be a route of entry for these relatively large compounds, as is the case for suramin (52).

Our data, showing an obvious cell cycle defect after treatment, with parasites becoming unable to correctly complete cell division and accumulating supernumerary kinetoplasts and nuclei and displaying an apparent fragmentation of nuclear material, are consistent with targeting of nuclear

DNA. This phenotype becomes manifest after a period of 12 to 24 hours, when it appears that the parasites in G1 phase (1K1N) are no longer able to enter the cell cycle. The exact causes of the cytokinesis block are still unclear but the combined evidence from the cell cycle experiments and the cellular distribution of the S-MGBs point to a potential multi-factorial mechanism of action, which would further delay the onset of resistance.

Metabolomics identified a significant accumulation of pyrimidines, particularly deoxyuridine, after 8 hours of treatment, hence supporting the hypothesis of S-MGBs interference with nucleic acids functions. In trypanosomes deoxyuridine is part of the pyrimidine salvage pathway: it is converted to dUMP (also significantly accumulating in treated cells), which is then converted into dTMP and the nucleoside triphosphate TTP used for DNA synthesis. From our results we could speculate that dUMP could accumulate as a result of downregulation of thymidylate synthase activity when DNA synthesis slows down, an hypothesis consistent with the absence of an accumulation of thymidine nucleotides despite an accumulation of other deoxynucleotides (dCTP, dAMP). This could generate high levels of dUTP, and its misincorporation into DNA, with consequent DNA damage. Previous work in *T. brucei* procyclic form found that addition of exogenous thymidine could alter the dTTP/dUTP ratio, reverting the inhibition of dUTPase (deoxyuridine triphosphate nucleotidohydrolase), the enzyme that provides the substrate for the thymidylate synthase and responsible for keeping the intracellular levels of dUTP low (53). However, we could not rescue bloodstream *T. brucei* grown in medium lacking thymidine and treated with **7** after addition of 10-20 mM of thymidine (data not shown).

Existing MGB drugs, such as diminazene, have been of enormous value for the treatment and control of trypanosomiasis since their introduction more than half a century ago, but are now failing as anti-parasitic therapeutics due to the significant rise of resistance. This study has demonstrated both the excellent *in vitro* activity and *in vivo* cure of parasitaemia by S-MGBs that are structurally distinct from existing MGB-based drugs. Specifically, in an *in vivo* model of infection of *T. congolense,* cures were demonstrate with either two applications of 50 mg/kg of **7** or two applications of 10 mg/kg of **8**. Moreover, S-MGBs have been shown to be unaffected by existing MGB-resistance mechanisms, both

in *T. congolense* and in *T. b. brucei*; in the latter this is due to a different mechanism of uptake in *T. brucei*. Furthermore, we found no indication of potential cross-resistance to the other class of veterinary trypanocides currently used in Africa: the phenanthridines isometamidium and ethidium. Finally, despite numerous efforts, selection of resistance to the S-MGBs *in vitro* proved unsuccessful, a result that could indicate a degree of refractoriness to resistance mechanisms of these compounds, likely linked to non-specific uptake and multifactorial trypanocidal actions. Together these observations provide proof of concept of S-MGBs as potential novel therapeutic agents for animal African trypanosomiasis.

Experimental Section

Trypanosomes and cell culture. Bloodstream form *T. congolense* strain IL3000 and derived diminazene-resistant lines were cultured at the University of Glasgow as described in (54), at 34 °C in a humidified, 5% CO_2 environment, in MEM medium (Sigma-Aldrich) supplemented with 25 mM HEPES, 26 mM $NaHCO_3$, 5.6 mM D-glucose, 1 mM sodium pyruvate, 40 μM adenosine, 100 μM hypoxanthine, 16.5 μM thymidine and 25 μM bathocuproinedisulfonic acid disodium salt. To this basal medium were added freshly prepared β-mercaptoethanol (0.0014% v/v), 1.6 mM glutamine, 100 units/ml penicillin, 0.1 mg/ml streptomycin, 20% goat serum (Gibco) and 5% Serum Plus (SAFC Biosciences). Bloodstream form *T. b. brucei* wild type (strain Lister 427) and derived lines were cultured at 37 °C in a humidified, 5% CO_2 environment in HMI-11 (Gibco), containing 10% FBS (Gibco). Kinetoplast-independent F_1-γ(L262P)-expressing trypanosomes were kindly provided by Dr Achim Schnaufer (University of Edinburgh) and grown in the presence of 2 μg/ml G418. The akinetoplastic version of γL262P, γL262P(AK), was obtained by exposure to 10 nM ethidium bromide for several passages. Loss of kinetoplast was verified by fluorescence microscopy of DAPI-stained cells. The origins of the trypanosome stocks (*T. congolense* IL3000 and STIB 736/IL1180 and *T. vivax* STIB 719/ILRAD 560 strains) and their respective culture media used at the Swiss TPH Institute, have been previously described in reference 37.

Generation of diminazene-resistant *T. congolense* lines. Bloodstream form *T. congolense* strain IL3000 was selected for diminazene resistance by subculturing cells *in vitro* in the continuous

presence of increasing concentration of diminazene. To enhance the chances of obtaining a resistant phenotype, some lines were mutagenized with 0.001% EMS for 90 min prior to selection with the drug. After two years, clones DimR (not mutagenized) and EMS MUT DimR (mutagenized with EMS) were generated, both growing in the presence of 800 nM diminazene, being 10- and 12-fold resistant, respectively relative to wild type.

***In vitro* and *ex vivo* trypanocidal activity and L6 toxicity.** The initial S-MGBs library screen against *T. congolense*, *T. vivax* and L6 cells (data presented in Table 1) was performed at the Swiss TPH Institute. To determine the EC_{50} values for the two trypanosome species specific modifications of the Alamar Blue assay (55) and the ^{3}H-hypoxanthine incorporation assay (56) were used, as previously described in (37). All experiments were performed in three independent assay runs for each compound.

To ascertain the cytotoxicity of each compound tested, the Alamar Blue assay (56) was followed, using an L6 (rat skeletal myoblast) cell line, but with minor modifications. The cell density was calculated using a Neubauer counting chamber and then diluted accordingly with culture medium, to obtain a seeding density of 2×10^4 cells/ml. The microtitre plates were then incubated overnight at 37 ºC and 5% CO_2, to enable the cells to adhere to the plates. The following day, the test compounds were added to the plates, using a three-fold serial dilution step across each plate, before being placed back into the incubator for 69 h under the same conditions. Thereafter, the plates were removed from the incubator and 10 µl of resazurin dye were placed into each well. The plates were incubated for a further 3 h, under the same conditions. After a total of 72 h incubation, the plates were removed and read using a fluorescence reader (SpectraMax, Gemini XS, Bucher Biotec, Basel, Switzerland) at an excitation wavelength of 536 nm and an emission wavelength of 588 nm. The EC_{50} values were determined using SOFTmax Pro 5.2 analysis software.

A modified Alamar Blue assay protocol was used to study S-MGBs cross-resistance in diminazene resistant *T. congolense* and *T. b. brucei* at the University of Glasgow. *T. b. brucei* (2×10^4 cell/ml) or *T. congolense* (2.5×10^5 cell/ml) cells were seeded into 96-well plates containing serial 2-fold dilutions

of test compounds. After 48 h incubation at (37 °C for *T. b. brucei* and 34 °C for *T. congolense*; 5% CO_2), 20 µl of resazurin dye solution (0.49 mM in PBS, Sigma-Aldrich) was added, and cells were incubated for a further 24 h before fluorescence was determined. Akinetoplastic *T. b. brucei* lines (ISMR1 and γL262P (AK)) were incubated with test compounds for 69 h, before addition of 10 µl of resazurin dye and readout after a further 3 h incubation. Resazurin reduction was measured with a fluorimeter (FLUOstar Optima, BMG Labtech) using 544 nm excitation and 590 nm emission wavelengths. Data were plotted to an equation for a sigmoid curve with variable slope in GraphPad Prism 5 software. All experiments were carried out on at least three independent occasions.

***In vivo* trypanocidal activity.** Pathogen-free (SPF) NMRI female mice (21-23 g) were used for all *in vivo* mouse trials within this study. Mice were housed in standard Macrolon Type II cages and were kept at a room temperature of 22 ºC and a relative humidity of 60-70%, receiving pelleted food and water *ad libitum*. All *in vivo* mouse trials were conducted in accordance with the regulations and guidelines set out by the Swiss Federal Veterinary Office, under License Number RB-739**.** For the *in vivo* mouse trials, a 50 mg/kg stock solution was prepared for each of the S-MGB test compounds, dissolved in sterile distilled water and containing no more than 10% DMSO. From these stock solutions, further dilutions were made depending on the dose being tested. All stock solutions and dilutions were made fresh on the day of administration and for each separate mouse trial. Mice were randomly selected and arranged into groups of four, before being independently infected intraperitoneally (i.p.) with 10^5 parasites in 0.25 ml of (6:4) phosphate buffered saline with glucose (PSG), using a drug-sensitive strain of *T. congolense* (STIB 736/IL1180). Infection of all *in vivo* mouse trials was performed from stabilated infected blood, stored frozen in liquid nitrogen, held within the cryobank of the Swiss TPH Institute. For all *T. congolense* mouse trials, a parasitaemia of 10^6 per ml blood was allowed to develop over 7 days, before compound treatment was administered (i.p.) on days 7 and 8 post infection (p.i.) (for 2 application regimens, 24 h apart) or days 7 to 10 p.i. (for 4 application regimens, 24 h apart). For single bolus dose applications, compound treatment (i.p.) was initiated on day 7 p.i. only. Subsequently, parasitaemia in mice was monitored using a tail blood examination technique, until day 60 post treatment to check for any possible relapses. Parasitaemia

was checked twice a week for the first 30 days and then once per week thereafter. At the end of the *in vivo* mouse trials, any surviving and aparasitaemic mice were considered cured. Untreated control mice survive, on average, 11 days p.i. using this infection protocol.

Fluorescence microscopy. *T. congolense* cells (5×10^5 cells/ml) were treated with highly fluorescent **9** or **16** ($2 \times EC_{50}$) for 2 - 48 h at 34 °C in a humidified 5% CO_2 atmosphere. For DAPI co-localisation, 20 μM of DAPI in water solution was added to the cultures 15 min before slide preparation. At set time points, cells were washed in PBS, and an aliquot of parasites was mixed with an equal volume of 2% w/v low melting point agarose (Sigma-Aldrich) and spread onto a slide by addition of a coverslip. Slides were viewed using a Zeiss Axioplan 2 Imaging epifluorescence microscope, equipped with a digital CCD camera (Hammatsu Photonics) and a PlanNEUFLUAR 100× oil-immersion NA 1.4 objective (Carl Zeiss). Standard FITC, GFP , DsRed and DAPI filters were used, and images were acquired using Volocity imaging software (Improvision). Images were merged using GIMP 2.10.4 software to overlay for co-localisation.

Time-to-kill assay. Killing kinetics curves for **7** were obtained by continuously exposing *T. b. brucei* (2×10^4 cell/ml) or *T. congolense* (1.25×10^5 cell/ml) to different doses of the compound. Cell densities were counted at set timepoints using a Neubauer haemocytometer. Three independent measurements were obtained for each condition.

Reversibility of trypanocidal effect. To determine the time required for **7** to cause irreversible effects on trypanosomes, an adaptation of a protocol published by Kaminsky *et al*. (57) was adopted. *T. b. brucei* (2×10^4 cell/ml) and *T. congolense* (2.5×10^5 cell/ml) were exposed to different doses of the compound, for set periods, under standard culture conditions. A pulse timepoint, where parasites were exposed to the compound and washed immediately after, was also included. Drug concentrations sufficient to kill at least 99.9% of cells determined from the EC_{50} curves were chosen for this experiment, but these had to be further increased to 10 and 20 fold EC_{50} to obtain cidal effect on *T. b. brucei*. At the designated times, cells were collected and washed twice in ice-cold medium to remove test compound. Parasites were finally resuspended in 1 ml of warm medium and cultivated in 24-well

plates. Parasites were then monitored daily for 15 days by light microscopy, to assess their ability to recover from transient exposure to the compound. All sets of conditions were assessed in triplicate. The veterinary drug diminazene was examined in parallel for comparison.

EdU incorporation assay. Direct measurement of DNA synthesis was performed using the Click-iT® EdU assay (Thermo Fisher Scientific) following manufacturers' instructions with some modifications. *T. b. brucei* (5×10^5 cell/ml), maintained in thymidine-free HMI-11 medium, were seeded in 24-well plates and treated with different concentrations of **7**, for 8 h under standard culture conditions. 5-ethynyl-2´-deoxyuridine (EdU) was added at a final concentration of 150 μM to each well, 4 h before the end of the treatment with test compound. Cells were then placed onto each well of a 12-spot microscope slide (Thermo Scientific) coated with poly-L-lysine, and allowed to adhere for 15 min at room temperature. After careful removal of the medium, trypanosomes were fixed with a 3.7% formaldehyde solution. After fixative removal, cells were washed with 1× PBS and then permeabilised for 30 min with a 0.1% Triton X-100 solution in 1× PBS. This was removed and the cells were washed twice with 1× PBS prior to the addition of 25 μl of a freshly prepared Click-iT® EdU detection mix (Thermo Fisher Scientific), containing the fluorophore Alexa Fluor 555 Azide. The mix was incubated with the cells for 1 h at room temperature, in a humidity chamber, protected from light. At the end of the incubation time, cells were washed 6 times with 1× PBS and finally counterstained with 4 μM DAPI and covered with a coverslip. Incorporation of the nucleoside analogue of thymidine, EdU, into newly synthesized DNA was visualised using a Zeiss Axioplan 2 imaging epifluorescence microscope, equipped with a digital CCD camera (Hammatsu Photonics) and a PlanNEUFLUAR 100× oil-immersion NA 1.4 objective (Carl Zeiss) using RHOD filter set. DMSO samples were prepared as negative controls, and aphidicolin (an inhibitor of eukaryotic nuclear DNA replication) (Sigma-Aldrich) was used as positive control at a dose of 1 μg/ml. All conditions were assessed in at least four independent occasions.

Cell cycle analysis. Nuclei/kinetoplast (N/K) configurations of **7**-treated *T. b. brucei* were monitored to assess effects on cell cycle progression. Trypanosomes (2×10^4 cell/ml) were treated either with different doses of test compound or DMSO as negative control and kept under standard culture

conditions in 24-well plates. At set timepoints (12, 24, 48 and 72 h), trypanosomes were collected, applied to a slide and allowed to dry. Slides were fixed overnight in cold methanol and kept at 4 °C after drying. Fixed cells were then rehydrated by adding 1-2 ml of PBS and, after eliminating the excess buffer, stained with 4 μM DAPI. A Zeiss Axioplan 2 Imaging epifluorescence microscope, equipped with a digital CCD camera (Hammatsu Photonics) and a PlanNEUFLUAR 100× oil-immersion NA 1.4 objective (Carl Zeiss) was used to view cells, using a standard DAPI filter set. Volocity imaging software (Improvision) was used for image acquisition. For each condition, the N/K configuration of at least 200 cells was recorded. Trypanosomes with configurations 3K1N, 1K3N (in which at least the N or the K had undergone two rounds of division in absence of cytokinesis), as well as cells with highly fragmented DNA-containing organelles were all included in the MKMN category. The experiment was carried out on three independent occasions.

Metabolomics analysis. Following treatment with test compound **7** at 2 × EC_{50} for 8 h under standard culture conditions (or to a corresponding volume of DMSO for the negative controls), *T. b. brucei* metabolites were extracted for untargeted metabolomics analysis. For each sample, 1 × 10^8 cells were collected and rapidly cooled to 4 °C by submersion of the tube in a dry ice-ethanol bath, to quench metabolism and denature proteins. Samples were kept at this temperature for all of the subsequent steps. Following centrifugation (1250 × *g*, 10 min), the supernatant was removed and the cell pellet was washed in 1 × PBS. The PBS was then removed and the cells lysed by resuspending in 200 μl of extraction solvent (chloroform:methanol:water 1:3:1). Metabolite extraction was obtained by vigorous shaking for 1 h at 4 °C. Extract mixture was then centrifuged at maximum speed and the supernatant collected and frozen at -80 °C under argon until LC-MS analysis. Four biological replicates were prepared for each condition.

Samples were analysed at the Glasgow Polyomics Metabolomics Facility using an Exactive Orbitrap mass spectrometer (Thermo Fisher) in both positive and negative modes (switching mode) and coupled to a HPLC system (Dionex) with a ZIC-pHILIC column (Merck SeQuant), as described before. Exactive data were acquired as previously described (58). Untargeted peak-picking and peak matching from raw LC-MS data were obtained using XCMS and mzMatch respectively. Metabolite

identification and relative quantitation was performed using the IDEOM interface (59), by matching accurate masses and retention times of authentic standards or, when standards were not available, by using predicted retention times. The putative metabolite list obtained by IDEOM was manually checked and filtered based on peak intensity and shape. Statistical analysis of the resulting list was performed using MetaboAnalyst 3.0 following log transformation of the data. Fragmentation patterns were integrated in the analysis using the Polyomics integrated Metabolomics Pipeline (PiMP) (60).

Transmission electron microscopy. *T. b. brucei* parasites (1×10^6 cells/ml) were treated with **7** ($2 \times EC_{50}$) for 8 h. Parasites were then collected, washed once in 1× PBS, and resuspended in fixative (2.5% glutaraldehyde plus 4% paraformaldehyde in 0.1 M PIPES, pH 7.3). After washing in 0.1 M sodium cacodylate buffer, cells were post-fixed in 1% osmium tetroxide for 1 h in the dark, washed in distilled water and stained with 0.5% aqueous uranyl acetate solution for 30 min in the dark. Parasites were then washed in distilled water and dehydrated in acetone solutions (30, 50, 70, 90, 100%). Cell were then embedded in epoxy resin (TAAB Laboratories Equipment Ltd). Ultrathin sections (50 nm) were sectioned using a Leica EM UC7 ultramicrotome, collected in Formvar-coated grids and visualised on a Jeol 1200 transmission electron microscope operating at 80 kV.

Compound synthesis. The details of previously published compounds can be found in the Supplementary Information. The following describes the synthesis of novel compounds.

Chemical reagents were obtained from Aldrich Chemical (Saint Louis, Missouri), Acros Organics, abcr GmBh (Karlsruhe, Germany), ACB Blocks (Toronto, Canada) and Chembridge, and were used without further purification. ^{1}H spectra were measured on a Bruker DPX-400 MHz spectrometer with chemical shifts given in ppm (δ-values), relative to proton and carbon traces in solvent. Coupling constants are reported in Hz. ^{13}C NMR are not reported due to synthesis of insufficient material and our experience of ^{13}C NMR spectra being uninformative in S-MGB characterisation due to significantly overlapping signals. IR spectra were recorded on a Perkin Elmer, 1 FT-IR spectrometer. Mass spectra were obtained on a Jeol JMS AX505. Anhydrous solvents were obtained from a Puresolv purification system, from Innovative

Technologies, or purchased as such from Aldrich. Chromatography was carried out using 200-400 mesh silica gels, or using reverse-phase HPLC on a waters system using a C18 Luna column. All final MGBs were of >95% purity as determined by HPLC.

HPLC method used for the purification of final MGBs:

Time (mins)	Flow rate (mL/min)	%Water (0.1%TFA)	%Acetonitrile (0.1%TFA)
0	6	90	10
25	6	60	40
35	6	50	50
40	6	30	70
44	6	90	10

5-{[(5-{[(5-{[(3-amino-3-iminiopropyl)amino]carbonyl}-1-methyl-1H-pyrrol-3-yl)amino]carbonyl}-1-methyl-1H-pyrrol-3-yl)amino]carbonyl}-2-[(E)-2-(4-methoxyphenyl)ethenyl]pyridinium bis(trifluoroacetate) 7

N-(5-{[(3-Amino-3-iminopropyl)amino]carbonyl}-1-methyl-1*H*-pyrrol-3-yl)-1-methyl-4-nitro-1*H*-pyrrole-2-carboxamide (61) (30 mg, 0.083 mmol) was dissolved in MeOH (3 mL) to which was added Pd/C-10 % (30 mg) and this was subjected to hydrogenation for 2 h at atmospheric pressure. After this, the reaction mixture was filtered through keisulghur and the solvent removed by rotary evaporation. The resulting residue was dissolved in dry DMF (1 mL) and to this was added 6-[(*E*)-2-(4-hydroxyphenyl)ethenyl]nicotinic acid (17) (21 mg, 0.083 mmol) and HBTU (64 mg, 0.17 mmol). The reaction mixture was left to stir overnight at room temperature and subjected to HPLC purification directly to yield the desired material as an off-white solid (21 mg, 32 %).

IR: 3295, 3094, 2935, 1677, 1655, 1640, 1612, 1578, 1558, 1543, 1530, 1472, 1433, 1408, 1386, 1261, 1196, 1183, 1134, 1064, 1013, 965 cm^{-1}

δ_H *NMR (DMSO-*d_6*):* 10.35 (1H, s), 9.95 (1H, s), 9.26 (1H, d, *J* = 2.0), 8.89 (2H, s), 8.54 (1H, m), 8.43 (2H, s), 8.19 (1H, m), 7.99-8.03 (4H, m), 7.59-7.82 (6H, m), 7.34 (1H, d, *J* =

1.5), 7.18 (1H, d, *J* = 1.5), 7.12 (1H, d, *J* = 1.5), 6.97 (1H, d, *J* = 1.5), 3.88 (3H, s), 3.82 (6H, s), 3.48-3.51 (2H, m), 2.58-2.62 (2H, m).

HR-MS-FAB: Found 569.2618 calculated for $C_{30}H_{33}O_4N_8^+$ (M+H) 569.2619.

1-amino-3-({[4-({[4-({4-[(E)-2-(3-methoxyphenyl)ethenyl]benzoyl}amino)-1-methyl-1H-pyrrol-2-yl]carbonyl}amino)-1-methyl-1H-pyrrol-2-yl]carbonyl}amino)-1-propaniminium trifluoroacetate 8

N-(5-{[(3-Amino-3-iminopropyl)amino]carbonyl}-1-methyl-1*H*-pyrrol-3-yl)-1-methyl-4-nitro-1*H*-pyrrole-2-carboxamide (61) (30 mg, 0.083 mmol) was dissolved in MeOH (3 mL) to which was added Pd/C-10 % (30 mg) and this was subjected to hydrogenation for 2 h at atmospheric pressure. After this, the reaction mixture was filtered through keisulghur and the solvent removed by rotary evaporation. The resulting residue was dissolved in dry DMF (1 mL) and to this was added 4-[(*E*)-2-(3-methoxyphenyl)ethenyl]benzoic acid (17) (21 mg, 0.083 mmol) and HBTU (64 mg, 0.17 mmol). The reaction mixture was left to stir overnight at room temperature and subjected to HPLC purification directly to yield the desired material as an off-white solid (22 mg, 39 %).

IR: 3295, 3068, 2948, 2824, 1703, 1673, 1655, 1632, 1614, 1582, 1561, 1546, 1532, 1513, 1502, 1489, 1470, 1436, 1403, 1390, 1276, 1198, 1174, 1121, 1051, 1008 cm^{-1}

δ_H NMR (DMSO-d_6): 10.31 (1H, s), 9.94 (1H, s), 8.89 (2H, s), 8.48 (2H, s), 8.19 (1H, t, *J* = 5.5), 7.95 (2H, d, *J* = 8.5), 7.73 (2H, d, *J* = 8.5), 7.29-8.37 (4H, m), 7.21-7.23 (2H, m), 7.18 (1H, d, *J* = 1.5), 7.10 (1H, d, *J* = 1.5), 6.95 (1H, d, *J* = 1.5), 6.88 (1H, m), 3.87 (3H, s), 3.81 (3H, s), 3.80 (3H, s), 3.48-3.51 (2H, m), 2.58-2.62 (2H, m).

HR-MS-FAB: Found 568.2672 calculated for $C_{31}H_{34}O_4N_7^+$ (M+H) 568.2667.

N-[5-({[5-({[2-(Dimethylamino)ethyl]amino}carbonyl)-1-methyl-1H-pyrrol-3-yl]amino}carbonyl)-1-methyl-1H-pyrrol-3-yl]-6-{(E)-2-[4-(dimethylamino)phenyl]ethenyl}nicotinamide 9

N-[2-(Dimethylamino)ethyl]-1-methyl-4-{[(1-methyl-4-nitro-1*H*-pyrrol-2-yl)carbonyl]amino}-1*H*-pyrrole-2-carboxamide (62) (0.160 g, 0.147 mmol) was dissolved in methanol (25 mL) to which Pd/C-10% (35 mg) was added at room temperature with stirring under nitrogen. The reaction mixture was hydrogenated at room temperature and atmospheric pressure for 2h. The catalyst was removed over Kieselguhr and methanol was removed under reduced pressure to give the amine which was dissolved in dry DMF (2 mL). 6-{(*E*)-2-[4-(dimethylamino)phenyl]ethenyl}nicotinic acid (20) (39 mg, 0.147 mmol) and HBTU (102 mg, 0.147 mmol) were added with stirring at room temperature. The reaction mixture was heated at 55^{o}C for 24h. HPLC purification of the reaction mixture gave the required product as a red solid material (44 mg, 52%) with no distinct melting point.

IR: 720, 804, 1128, 1175, 1287, 1366, 1435, 1528, 1576, 1668 cm^{-1}

δ_H *NMR (DMSO-d_6):* 10.45 (1H, s), 9.98 (1H, s), 9.27 (1H, br), 9.04 (1H, s), 8.25 (1H, dd, *J* = 2.85, 13.0), 8.19 (1H, t, J = 8.9), 7.72 (1H, d, J = 16.0), 7.64 (1H, d, J = 8.3), 7.54 (2H, d, J = 8.9), 7.34 (1H, d, *J* = 1.5), 7.21 (1H, d, *J* = 1.5), 7.10-7.15 (2H, m), 7.01 (1H, d, *J* = 1.5), 6.76 (2H, d, J = 8.9), 3.89 (3H, s), 3.84 (3H, s), 3.52 (2H, q, *J* = 6.0), 3.23 (2H, q, *J* = 6.0), 2.99 (6H, s), 2.85 (6H, m).

HR-MS-FAB: found: 583.3144 calculated for $C_{32}H_{38}N_8O_3$ 583.3145

N-[2-(Dimethylamino)ethyl]-4-({[4-({4-[(E)-2-(3-methoxyphenyl)ethenyl]benzoyl}amino)-1-methyl-1H-pyrrol-2-yl]carbonyl}amino)-1-methyl-1H-pyrrole-2-carboxamide 10

N-[2-(Dimethylamino)ethyl]-1-methyl-4-{[(1-methyl-4-nitro-1*H*-pyrrol-2-yl)carbonyl]amino}-1*H*-pyrrole-2-carboxamide (62) (0.160 g, 0.147 mmol) was dissolved in methanol (25 mL) to which Pd/C-10% (35 mg) was added at room temperature with stirring under nitrogen. The reaction mixture was hydrogenated at room temperature and atmospheric pressure for 2h. The catalyst was removed over Kieselguhr and methanol was removed under reduced pressure to give the amine which was dissolved in dry DMF (2 mL). 4-[(*E*)-2-(3-methoxyphenyl)ethenyl]benzoic acid (17) (38 mg, 0.147 mmol) and HBTU (102 mg, 0.147 mmol) were added with stirring at room temperature. The reaction mixture was heated at 55^{o}C for 24h. HPLC purification of the reaction mixture gave the required product as pale yellow solid material (30 mg, 36%) with no distinct melting point.

IR: 689, 777, 976, 1134, 1165, 1198, 1262, 1402, 1433, 1464, 1514, 1580, 1641 cm^{-1}

δ_H *NMR (DMSO-d$_6$):* 10.32 (1H, s), 9.96 (1H, s), 9.28 (1H, br), 8.183 (1H, t, *J* = 5.6), 7.96 (2H, d, *J* = 8.4), 7.73 (2H, d, *J* = 8.4), 7.28-7.40 (4H, m), 7.18-7.22 (3H, m), 7.11 (1H, d, *J* = 1.5), 7.00 (1H, d, *J* = 1.5), 6.88 (1H, dd, *J* = 3.7, *J* = 1.5), 3.87 (3H, s), 3.83 (3H, s), 3.81 (3H, s), 3.51 (2H, q, *J* = 6.0), 3.21 (2H, q, *J* = 6.0), 2.84 (6H, m).

HR-MS-FAB: found: 569.2880 calculated for $C_{32}H_{36}N_6O_4$ 569.2876

N-[2-(Dimethylamino)ethyl]-1-methyl-4-({[1-methyl-4-({4-[(E)-2-(3-quinolinyl)ethenyl]benzoyl}amino)-1H-pyrrol-2-yl]carbonyl}amino)-1H-pyrrole-2-carboxamide 11

N-[2-(Dimethylamino)ethyl]-1-methyl-4-{[(1-methyl-4-nitro-1*H*-pyrrol-2-yl)carbonyl]amino}-1*H*-pyrrole-2-carboxamide (62) (0.160 g, 0.147 mmol) was dissolved in methanol (25 mL) to which Pd/C-10% (35 mg) was added at room temperature with stirring under nitrogen. The reaction mixture was hydrogenated at room temperature and atmospheric pressure for 2h. The catalyst was removed over Kieselguhr and methanol was removed under

reduced pressure to give the amine which was dissolved in dry DMF (2 mL). 4-[(*E*)-2-(3-quinolinyl)ethenyl]benzoic acid (17) (41 mg, 0.147 mmol) and HBTU (102 mg, 0.147 mmol) were added with stirring at room temperature. The reaction mixture was left stirring at room temperature for 24h. HPLC purification of the reaction mixture gave the required product as yellow solid material (14 mg, 14%) with no distinct melting point.

IR: 720, 831, 972, 1061, 1128, 1196, 1267, 1414, 1431, 1495, 1539, 1624, 1674 cm^{-1}

δ_H NMR (DMSO-d_6): 10.35 (1H, s), 9.97 (1H, s), 9.26 (2H, b), 8.56 (1H, d, *J* = 2.0), 8.18 (1H, t, *J* = 6.0), 7.98-8.04 (4H, m), 7.81 (2H, d, *J* = 9.0), 7.76 (1H, t, *J* = 6.5), 7.6-7.7 (3H, m), 7.33 (1H, d, *J* = 2.0), 7.20 (1H, d, *J* = 2.0), 7.12 (1H, d, *J* = 2.0), 7.00 (1H, d, *J* = 2.0), 3.88 (3H, s), 3.83 (3H, s), 3.51 (2H, q, *J* = 6.0), 3.23 (2H, q, *J* = 6.0), 2.84 (6H, m).

HR-MS-FAB: found: 590.2882 calculated for $C_{34}H_{35}N_7O_3$ 590.2880

5,6-Dichloro-N-[5-({[5-({[4-({[3-(dimethylamino)propyl]amino}carbonyl)-5-isopropyl-1,3-thiazol-2-yl]amino}carbonyl)-1-methyl-1H-pyrrol-3-yl]amino}carbonyl)-1-methyl-1H-pyrrol-3-yl]nicotinamide 17

N-[3-(Dimethylamino)propyl]-5-isopropyl-2-{[(1-methyl-4-{[(1-methyl-4-nitro-1*H*-pyrrol-2-yl)carbonyl]amino}-1*H*-pyrrol-2-yl)carbonyl]amino}-1,3-thiazole-4-carboxamide (90 mg, 0.165 mmol) was dissolved in methanol (25), then it was cooled to 0°C and Pd/C-10% (82 mg) was added portionwise under N_2 with stirring. The reaction mixture was hydrogenated at room temperature and atmospheric pressure for 6h. The catalyst was removed over Kieselguhr and the solvent was removed under reduced pressure. 5,6-Dichloronicotinic acid (32 mg, 0.165 mmol) was dissolved in thionyl chloride (2 mL) and heated under reflux for 2h. Excess thionyl chloride was removed under reduced pressure and the residue was dissolved in dry DCM (5 mL). The amine was dissolved in dry DCM (5mL) to which NMM (0.5 mL) was added followed by the acid chloride solution. The stirring was continued at

room temperature overnight. The volatile material was removed under reduced pressure and the crude product was purified by HPLC. Fractions containing the required material were collected and freeze dried to give the pure product as light brown solid (66 mg, 50%) with no distinct melting point.

IR: 1660, 1548, 1466, 1284, 1201, 1129, 774, 721 cm^{-1}.

δ_H *NMR (DMSO-d_6):* 12.05(1H, s), 10.68(1H, s), 10.11(1H, s), 9.32(1H, br), 8.89(1H, d, J=2.4Hz), 8.59(1H, d, J=2.5Hz), 7.96(1H, t, unresolved), 7.45(1H, d, J=1.6Hz), 7.40(1H, d, J=1.6Hz), 7.36(1H, d, J=1.6Hz), 7.13(1H, d, J=1.6Hz), 4.20(1H, quintet, J=6.8Hz), 3.89(6H, s), 3.35(2H, q, J=6.4Hz), 3.06(2H, m), 2.79(6H, d, J=4.7Hz), 1.87(2H, q, unresolved), 1.29(6H, d, J=6.8Hz).

HR-MS-FAB: found: 688.2017 calculated for $C_{30}H_{36}N_9O_4S^{35}Cl_2$ 688.1988.

4-(Ethanimidoylamino)-1-methyl-N-[1-methyl-5-({[1-methyl-5-({[2-(4-morpholinyl)ethyl]amino}carbonyl)-1H-pyrrol-3-yl]amino}carbonyl)-1H-pyrrol-3-yl]-1H-pyrrole-2-carboxamide 18

1-Methyl-*N*-[1-methyl-5-({[1-methyl-5-({[2-(4-morpholinyl)ethyl]amino}carbonyl)-1*H*-pyrrol-3-yl]amino}carbonyl)-1*H*-pyrrol-3-yl]-4-nitro-1*H*-pyrrole-2-carboxamide (56 mg, 0.106 mmol) was dissolved in methanol (25 mL) to which Pd/C-10% (29 mg) was added at 0^oC under N_2 with stirring. The reaction mixture was hydrogenated for 6h at room temperature and atmospheric pressure. The catalyst was removed over Kieselguhr. To the methanolic solution of the amine, methyl ethanimidothioate hydroiodide (23 mg, 0.106 mmol) was added at room temperature with stirring. The solution was left standing at room temperature for 48h. HPLC purification gave the product as white solid (32 mg, 39%) with no distinct melting point.

IR: 1665, 1550, 1290, 1200, 1131 $cm.^{-1}$

δ_H *NMR (DMSO-d_6):* 10.84(1H, s), 9.97(1H, s), 9.93(1H, s), 9.72(1H, br), 9.42(1H, s), 8.35(1H, s), 8.22(1H, s), 7.24(1H, d, J=1.7Hz), 7.19(1H, d, J=1.7Hz), 7.16(1H, d, J=1.7Hz), 7.06(1H, d, J=1.7Hz), 5.99(1H, d, J=1.7Hz), 6.92(1H, d, J=1.7Hz), 3.98(2H, m), 3.91(3H, s), 3.85(3H, s), 3.82(3H, s), 3.71-3.13(10H, m), 2.29(3H, s).

HR-MS-FAB: found: 538.2881 calculated for $C_{26}H_{36}N_9O_4$ 538.2890

N-[5-({[5-({[5-Isopropyl-4-({[2-(4-morpholinyl)ethyl]amino}carbonyl)-1,3-thiazol-2-yl]amino}carbonyl)-1-methyl-1H-pyrrol-3-yl]amino}carbonyl)-1-methyl-1H-pyrrol-3-yl]-3-isoquinolinecarboxamide 19

5-isopropyl-2-{[(1-methyl-4-{[(1-methyl-4-nitro-1*H*-pyrrol-2-yl)carbonyl]amino}-1*H*-pyrrol-2-yl)carbonyl]amino}-*N*-[2-(4-morpholinyl)ethyl]-1,3-thiazole-4-carboxamide (38 mg, 0.066 mmol) was dissolved in methanol (25 mL) to which Pd/C-10% (40 mg) was added at 0^{o}C under N_2 with stirring. The reaction mixture was hydrogenated for 5h at room temperature and atmospheric pressure. The catalyst was removed over Kieselguhr. Methanol was removed under reduced pressure at 50^{o}C and the amine so formed was dissolved in dry DMF (1 mL) to which NMM (40 µL) was added at room temperature with stirring followed by 3-isoquinolinecarboxylic acid (12 mg, 0.070) and HBTU (52 mg, 0.140 mmol). The stirring was continued at room temperature overnight. The product was obtained as white solid (25 mg, 36%) with no distinct melting point (after the purification by HPLC).

IR: 1662, 1545, 1276, 1200 cm.$^{-1}$

δ_H *NMR (DMSO-d_6):* 12.00(1H, s), 10.83(1H, s), 10.08(1H, s), 9.60(1H, br), 9.45(1H, s), 8.64(1H, s), 8.30(1H, d, J=7.7Hz), 8.24(1H, d, J=7.7Hz), 8.10(1H, t, J=6.0Hz), 7.92(1H, dt, J=1.6Hz & 7.0Hz), 7.85(1H, dt, J=1.6Hz & 7.0Hz), 7.45(2H, d, J=1.7Hz), 7.41(1H, d, J=1.7Hz), 7.33(1H, d, J=1.7Hz), 4.20(1H, septet, J=6.9Hz), 3.99-3.93(2H, m), 3.905(3H, s), 3.901(3H, s), 3.66-3.12(10H, m), 1.30(6H, d, J=6.9Hz).

HR-MS-FAB: found: 698.2867 calculated for $C_{35}H_{40}O_5N_9S$ 698.2873.

4-[(4-{(E)-2-[2-(1H-1,2,3-Benzotriazol-1-yloxy)-3-quinolinyl]ethenyl}benzoyl)amino]-1-methyl-N-[1-methyl-5-({[2-(4-morpholinyl)ethyl]amino}carbonyl)-1H-pyrrol-3-yl]-1H-pyrrole-2-carboxamide 20

1-Methyl-*N*-[1-methyl-5-({[2-(4-morpholinyl)ethyl]amino}carbonyl)-1*H*-pyrrol-3-yl]-4-nitro-1*H*-pyrrole-2-carboxamide (50 mg, 0.124 mmol) was dissolved in methanol (25 mL) to which was added Pd/C-10% (50 mg) at 0°C (under N_2) with stirring. The reaction mixture was hydrogenated for 3h at room temperature and atmospheric pressure. The catalyst was removed over Kieselguhr and the methanol was removed under reduced pressure. The amine so formed was dissolved in dry DMF (1 mL). To the amine solution the following were added: 4-[(*E*)-2-(2-chloro-3-quinolinyl)ethenyl]benzoic acid (38 mg, 0.124 mmol) and HBTU (94 mg, 0.248 mmol) and the reaction mixture was kept stirring overnight. The product was purified by HPLC (no work up required) to give the required product as a yellow solid after freeze drying (19 mg, 17%) with no distinct melting point.

IR: 1681, 1642, 1581, 1540, 1464, 1435, 1404, 1266, 1202, 1134 cm.$^{-1}$

δ_H NMR (DMSO-d_6): 10.39(1H, s), 9.97(1H, s), 9.55(1H, s), 9.03(1H, s), 8.24(2H, d, J=8.3Hz), 8.08-8.02(3H, m), 7.93-7.89(2H, m), 7.85-7.77(3H, m), 7.66-7.54(4H, m), 7.37(1H, d, J=7.8Hz), 7.34(1H, d, J=1.6Hz), 7.21(1H, d, J=1.6Hz), 7.14(1H, d, J=1.6Hz), 7.01(1H, d, J=1.6Hz), 4.02(2H, m), 3.88(3H, s), 3.86(3H, s), 3.69-3.53(6H, m), 3.27-3.14(4H, m).

HR-MS-FAB: Found: 765.3267 calculated for $C_{42}H_{41}N_{10}O_5$ 765.3261.

2-[({4-[(4-{(E)-2-[2-(1H-1,2,3-benzotriazol-1-yloxy)-3-quinolinyl]ethenyl}benzoyl)amino]-1-methyl-1H-pyrrol-2-yl}carbonyl)amino]-5-isopentyl-N-[2-(4-morpholinyl)ethyl]-1,3-thiazole-4-carboxamide 21

5-Isopentyl-2-{[(1-methyl-4-nitro-1*H*-pyrrol-2-yl)carbonyl]amino}-*N*-[2-(4-morpholinyl)ethyl]-1,3-thiazole-4-carboxamide: (80 mg, 0.167 mmol) was dissolved in methanol (25 mL) to which was added Pd/C-10% (60 mg) at 0°C (under N_2) with stirring. The reaction mixture was hydrogenated for 4h at room temperature and atmospheric pressure. The catalyst was removed over Kieselguhr and the methanol was removed under reduced pressure. The amine so formed was dissolved in dry DMF (2 mL). To the amine solution the following were added: 4-[(*E*)-2-(2-chloro-3-quinolinyl)ethenyl]benzoic acid (46 mg, 0.167 mmol) and HBTU (126 mg, 0.334 mmol) and the reaction mixture was kept stirring at room temperature overnight. The product was purified by HPLC (no work up required) to give the required product as a yellow solid after freeze drying (19 mg, 12%) with no distinct melting point.

IR: 1663, 1551, 1502, 1401, 1288, 1202, 1137, 778, 750 $cm.^{-1}$

δ_H NMR (DMSO-d_6): 12.09(1H, s), 10.49(1H, s), 9.68(1H, br), 9.03(1H, s), 8.93(1H, s), 8.23(1H, d, J=8.4Hz), 8.09-7.95(6H, m), 7.90-7.77(6H, m), 7.70(1H, t, J=7.0Hz), 7.65-7.57(4H, m), 7.55(1H, d, J=1.6Hz), 7.46(1H, d, J=1.6Hz), 7.37(1H, d, J=9.1Hz), 12.08(1H, s), 10.49(1H, s), 9.72(1H, br), 9.03(1H, s), 8.24(1H, d, J=8.4Hz), 8.08-7.99(3H, m), 7.94-7.88(1H, m), 7.85-7.79(2H, m), 7.66-7.56(3H, m), 7.54(1H, d, J=1.6Hz), 7.46(1H, d, J=1.6Hz), 7.37(1H, d, J=7.9Hz), 4.02(2H, m), 3.93(3H, s), 3.70-3.54(6H, m), 3.31-3.15(6H, m), 1.64-1.51(3H, m), 0.93(6H, d, J=6.3Hz).

HR-MS-FAB: Found: 839.3455 calculated for $C_{45}H_{47}O_5N_{10}S$ 839.3452.

Acknowledgements

We are very grateful to Dr Catarina Gadelha (University of Nottingham) for her valuable and insightful comments on the electron microscopy images. We are also thankful to Dr Achim Schnaufer (University of Edinburgh) for sharing with us his akinetoplastic *T. brucei* cell lines.

This research is part funded by the MSD Scottish Life Sciences fund. The opinions expressed in this research are those of the authors and do not represent those of MSD, nor its Affiliates. Funding was also provided by BBSRC grant BB/N007638/1.

Author contributions

K.G. carried out the *in vitro* experiments yielding the data in tables 1 and S1, and performed the *in vivo* experiments and analysed the data. F.G. carried out all other *in vitro* experiments and analysed the data. J.C.M. generated the diminazene-resistant *T. congolense* lines. A.I.K. and F.J.S. carried out the chemical synthesis and characterisation. F.G., K.G., C.J.S., and F.J.S. prepared the manuscript and all authors contributed to editing the paper.

Supporting Information Availability

Full panel of compounds and screening data; additional cross-resistance data; additional metabolomics data; additional toxicity vs activity plots (DOCX)

Molecular formula strings and some data (CSV)

Abbreviations Used

AAT animal African trypanosomiasis

HAT human African trypanosomiasis

MGB minor groove binder

S-MGB Strathclyde-minor groove binder

MKMN multiple kinetoplasts and nuclei

EdU 5-ethynyl-2′-deoxyuridine

References

1. Auty, H.; Torr, S. J.; Michoel, T.; Jayaraman, S.; Morrison, L. J. Cattle trypanosomosis: the diversity of trypanosomes and implications for disease epidemiology and control. *Rev. Sci. Tech.* **2015**, *34*, 587-598.

2. Grady, S. C.; Messina J. P.; McCord, P. F. Population vulnerability and disability in Kenya's tsetse fly habitats. *PLoS Negl. Trop. Disease.* **2011**, *5*, e957.

3. Giordani, F.; Morrison, L. J.; Rowan, T. G.; De Koning, H. P.; Barrett, M. P. The animal trypanosomiases and their chemotherapy: a review. *Parasitology*. **2016**, *143*, 1862-1889.

4. Clausen, P. H.; Sidibe, I.; Kabore, I.; Bauer, B. Development of multiple drug resistance of *Trypanosoma congolense* in Zebu cattle under high natural tsetse fly challenge in the pastoral zone of Samorogouan, Burkina Faso. *Acta. Trop.* **1992**, *51*, 229-236.

5. McDermott, J.; Woitag, T.; Sidibe, I.; Bauer, B.; Diarra, B.; Ouedraogo, D.; Kamuanga, M.; Peregrine, A.; Eisler, M.; Zessin, K. H.; Mehlitz, D.; Clausen, P. H. Field studies of drug-resistant cattle trypanosomes in Kenedougou Province, Burkina Faso. *Acta. Trop.* **2003**, *86*, 93-103.

6. Mungube, E. O.; Vitouley, H. S.; Allegye-Cudjoe, E.; Diall, O.; Boucoum, Z.; Diarra, B.; Sanogo, Y.; Randolph, T.; Bauer, B.; Zessin, K. H.; Clausen, P. H. Detection of multiple drug-resistant *Trypanosoma congolense* populations in village cattle of south-east Mali. *Parasit. Vectors.* **2012**, *5*, 155.

7. Delespaux, V.; Geysen, D.; Van den Bossche, P.; Geerts, S. Molecular tools for the rapid detection of drug resistance in animal trypanosomes. *Trends in Parasitology.* **2008**, *24*, 236–242.

8. Geerts, S.; Holmes, P. H.; Eisler, M. C.; Diall, O. African bovine trypanosomiasis: the problem of drug resistance. *Trends Parasitol.* **2001**, *17*, 25-28.

9. Tidwell, R. R.; Boykin, D. W. Dicationic DNA minor groove binders as antimicrobial agents. In *DNA and RNA Binders: From Small Molecules to Drugs*; Demeunynck, M., Bailly, C., Wilson, W. D., Eds.; 2002; Vol. 1, pp 414–460.

10. Wilson, W. D.; Nguyen, B.; Tanious, F. A.; Mathis, A.; Hall, J. E.; Stephens, C. E.; Boykin, D. W. Dications that target the DNA minor groove: compound design and preparation, DNA interactions,

cellular distribution and biological activity. *Curr. Med. Chem. - Anti-Cancer Agents.* **2005**, *5*, 389–408.

11. Wilson, W. D.; Tanious, F. A.; Mathis, A.; Tevis, D.; Hall, J. E.; Boykin, D. W. Antiparasitic compounds that target DNA. *Biochimie.* **2008**, *90*, 999–1014.

12. Thuita, J. K.; Karanja, S. M.; Wenzler, T.; Mdachi, R. E.; Ngotho, J. M.; Kagira, J. M.; Tidwell, R.; Brun, R. Efficacy of the diamidine DB75 and its prodrug DB289, against murine models of human African trypanosomiasis. *Acta Trop.* **2008**, *108*, 6-10.

13. Wenzler, T.; Boykin, D. W.; Ismail, M. A.; Hall, J.E.; Tidwell, R. R.; Brun, R. New treatment option for second-stage African sleeping sickness: *in vitro* and *in vivo* efficacy of aza analogs of DB289. *Antimicrob Agents Chemother*. **2009**, *53*, 4185-4192.

14. Paine, M. F.; Wang, M. Z.; Generaux, C. N.; Boykin, D. W.; Wilson, W. D.; De Koning, H. P.; Olson, C. A.; Pohlig, G.; Burri, C.; Brun, R.; Murilla, G. A.; Thuita, J. K.; Barrett, M. P.; Tidwell, R. R. Diamidines for human African trypanosomiasis. *Curr. Opin. Investig. Drugs*. **2010**, *11*, 876–883.

15. Graf, F.E.; Ludin, P.; Arquint, C.; Schmidt, R. S.; Schaub, N.; Kunz-Renggli, C.; Munday, J. C.; Krezdorn, J.; Baker, N.; Horn, D.; Balmer, O.; Caccone, A.; De Koning, H. P.; Mäser, P. Comparative genomics of drug resistance of the sleeping sickness parasite *Trypanosoma brucei rhodesiense*. *Cell Mol Life Sci.* **2016**, *73*, 3387-3400.

16. Khalaf, A. I.; Waigh, R. D.; Drummond, A. J.; Pringle, B.; McGroarty, I.; Skellern, G. G.; Suckling, C. J. Distamycin analogues with enhanced lipophilicity *J. Med. Chem.* **2004**, *47*, 2133-2156.

17. Suckling, C. J.; Breen, D.; Khalaf, A. I.; Ellis, E.; Hunter, I. S.; Ford, G.; Gemmell, C. G.; Anthony, N. G.; Helsebeux, J. -J.; Mackay, S. P.; Waigh R. D. Antimicrobial lexitropsins containing amide, amidine, and alkene linking groups. *J. Med. Chem.* **2007**, *50*, 6116-6125.

18. Scott, F. J.; Khalaf, A. I.; Avery, V. M.; Duffy, S.; Suckling, C. J. Selective anti-malarial minor groove binders. *Bioorg. Med. Chem. Lett.* **2016**, *26*, 3326-3329.

19. MGB Biopharma Home Page. http://www.mgb-biopharma.com/mgb-biopharma-successfully-completes-phase-i-clinical-trial-with-oral-mgb-bp-3-a-truly-novel-antibiotic-targeting-clostridium-difficile-infections/ (accessed Jan 9, 2019)

20. Barrett, M. P.; Gemmell, C. G.; Suckling, C. J. Minor groove binders as anti-infective agents. *Pharmacology & Therapeutics.* **2013**, *139,* 12-23.

21. Scott, F. J.; Khalaf, A. I, Giordani, F.; Wong, P. E.; Duffy, S.; Barrett, M.; Avery, V. M.; Suckling, C. J. An evaluation of minor groove binders as anti-*Trypanosoma brucei brucei* therapeutics. *Eur. J. Med. Chem*. **2016**, *116*, 116-125.

22. Alniss, H. Y.; Salvia, M. V.; Sadikov, M.; Golovchenko, I.; Anthony, N. G.; Khalaf, A. I.; MacKay, S. P.; Suckling, C. J.; Parkinson, J. A. Recognition of the DNA minor groove by thiazotropsin analogues. *Chem. BioChem.* **2014**, *15*, 1978-1990.

23. Bray, P. G.; Barrett, M. P.; Ward, S. A.; De Koning, H. P. Pentamidine uptake and resistance in pathogenic protozoa. *Trends Parasitol*. **2003**, *19*, 232-239.

24. Munday, J. C.; Eze, A. A.; Baker, N.; Glover, L.; Clucas, C.; Aguinaga Andrés, D.; Natto, M. J.; Teka, I. A.; McDonald, J.; Lee, R. S.; Graf, F. E.; Ludin, P.; Burchmore, R. J.; Turner, C. M.; Tait, A.; MacLeod, A.; Mäser, P.; Barrett, M. P.; Horn, D.; De Koning, H. P. *Trypanosoma brucei* Aquaglyceroporin 2 is a high affinity transporter for pentamidine and melaminophenyl arsenic drugs and is the main genetic determinant of resistance to these drugs. *J Antimicrob Chemother.* **2014**, *69*, 651-663.

25. Graf, F. E.; Baker, N.; Munday, J. C.; De Koning, H. P.; Horn, D.; and Mäser, P. Chimerization at the *AQP2-AQP3* locus is the genetic basis of melarsoprol-pentamidine cross-resistance in clinical *Trypanosoma brucei gambiense* isolates. *Int. J. Parasitol. Drugs Drug Res.* **2015**, *5*, 65-68.

26. Matovu, E.; Stewart, M. L.; Geiser, F.; Brun, R.; Maser, P.; Wallace, L. J.; Burchmore, R. J.; Enyaru, J. C.; Barrett, M. P.; Kaminsky, R.; Seebeck, T.; de Koning, H. P. Mechanisms of arsenical and diamidine uptake and resistance in *Trypanosoma brucei*. *Eukaryot Cell.* **2003**, *2*, 1003-1008.

27. De Koning, H. P.; Anderson, L. F.; Stewart, M.; Burchmore, R. J. S.; Wallace, L. J. M.; & Barrett, M. P. The trypanocide diminazene aceturate is accumulated predominantly through the TbAT1 purine transporter; additional insights in diamidine resistance in African trypanosomes. *Antimicrob Agents Chemother.* **2004**, *48*, 1515-1519.

28. Ward, C. P.; Wong, P. E.; Burchmore, R. J.; De Koning, H. P.; Barrett, M. P. Trypanocidal furamidine analogues: influence of pyridine nitrogens on trypanocidal activity, transport kinetics and resistance patterns. *Antimicrob Agents Chemother.* **2011**, *55*, 2352-2361.

29. Bridges, D. J.; Gould, M. K.; Nerima, B.; Maser, P.; Burchmore, R. J.; De Koning, H. P. Loss of the high-affinity pentamidine transporter is responsible for high levels of cross-resistance between arsenical and diamidine drugs in African trypanosomes. *Mol. Pharmacol.* **2007**, *71*, 98-108.

30. Baker, N.; Glover, L.; Munday, J. C.; Aguinaga, A. D.; Barrett, M. P.; De Koning, H. P.; Horn, D. Aquaglyceroporin 2 controls susceptibility to melarsoprol and pentamidine in African trypanosomes. *Proc. Natl. Acad. Sci. USA.* **2012**, *109*, 10996-11001.

31. De Koning, H. P.; MacLeod, A.; Barrett, M. P.; Cover, B.; Jarvis, S. M. Further evidence for a link between melarsoprol resistance and P2 transporter function in African trypanosomes. Mol Biochem Parasitol. **2000**, *106*, 181-185.

32. Munday, J. C.; Rojas Lopez, K. E.; Eze, A. A.; Delespaux, V.; Van Den Abbeele, J.; Rowan, T. Barrett, M. P.; Morrison, L. J.; de Koning, H. P. Functional expression of TcoAT1 reveals it to be a P1-type nucleoside transporter with no capacity for diminazene uptake. *Int. J. Parasitol. Drugs Drug Resist.* **2013**, *3*, 69-76.

33. Barrett, M. P.; Zhang, Z. Q.; Denise, H.; Giroud, C.; Baltz, T. A diamidine-resistant *Trypanosoma equiperdum* clone contains a P2 purine transporter with reduced substrate affinity.
Mol Biochem Parasitol. **1995**, *73*, 223-229.

34. Suswam, E. A.; Ross, C. A.; Martin, R.J. Changes in adenosine transport associated with melaminophenyl arsenical (Mel CY) resistance in *Trypanosoma evansi*: down-regulation and affinity changes of the P2 transporter. *Parasitology* **2003**, *127*, 543-549.

35. Graf, F. E.; Ludin, P.; Wenzler, T.; Kaiser, M.; Brun, R.; Pyana, P.; Büscher, P.; de Koning, H. P.; Horn, D.; Mäser, P. Aquaporin 2 mutations in *Trypanosoma b. gambiense* field isolates correlate with decreased susceptibility to pentamidine and melarsoprol. *PLoS Negl Trop Dis*. **2013**, *7*, e2475.

36. Graf, F. E.; Ludin, P.; Arquint, C.; Schmidt, R. S.; Schaub, N.; Kunz-Renggli, C.; Munday, J. C.; Krezdorn, J.; Baker, N.; Horn, D.; Balmer, O.; Caccone, A.; de Koning, H. P.; Mäser, P. Comparative

genomics of drug resistance of the sleeping sickness parasite *Trypanosoma brucei rhodesiense. Cell Mol Life Sci.* **2016**, *73*, 3387-3400.

37. Gillingwater, K.; Kunz, C.; Braghiroli, C.; Boykin, D. W. , Tidwell, R. R.; Brun, R.. *In vitro*, *ex vivo* and *in vivo* activity of diamidines against *Trypanosoma congolense* and *Trypanosoma vivax*. *Antimicrob Agents Chemother.* **2017**, *61*, e02356-16.

38. Dean, S.; Gould, M. K.; Dewar, C. E.; Schnaufer, A. C. Single point mutations in ATP synthase compensate for mitochondrial genome loss in trypanosomes. *Proc Natl Acad Sci USA.* **2013**, *110*, 14741-14746.

39. Eze, A. A.; Gould, M. K.; Munday, J. C.; Tagoe, D. N. A.; Stelmanis, V.; Schnaufer, A.; De Koning, H. P. Loss of mitochondrial membrane potential is a late adaptation of *Trypanosoma brucei brucei* to Isometamidium preceded by mutations in the γ Subunit of the F_1F_0-ATPase. *PLoS Negl Trop Dis.* **2016**, *10*, e0004791.

40. Gould, M. K.; Schnaufer, A. Independence from Kinetoplast DNA maintenance and expression is associated with multidrug resistance in *Trypanosoma brucei in vitro*. *Antimicrob Agents Chemother.* **2014**, *58*, 2925-2928.

41. Hammarton, T. C. Cell cycle regulation in *Trypanosoma brucei*. *Mol Biochem Parasitol.* **2007**, *153*, 1-8.

42. Mutomba, M. C.; Wang, C. C. Effects of aphidicolin and hydroxyurea on the cell cycle and differentiation of *Trypanosoma brucei* bloodstream forms. *Mol Biochem Parasitol.* **1996**, *80*, 89-102.

43. De Koning, H. P.; Gould, M. K.; Sterk, G. J.; Tenor, H.; Kunz, S.; Luginbuehl, E.; Seebeck, T. Pharmacological validation of *Trypanosoma brucei* phosphodiesterases as novel drug targets. *J Infect Dis.* **2012**, *206*, 229-237.

44. Suckling, C. J.; Hunter, I.; Khalaf, A. I.; Scott, F.; Tucker, N.; Niemenen, L.; Lemonidis, K. Why antibacterial minor groove binders are a good thing, *Proceedings of the 3rd International Electronic Conference on Medicinal Chemistry*, November 1, 2017.
https://sciforum.net/paper/view/conference/4651

45. Scott, F. J.; Nichol, R. J. O.; Khalaf, A. I.; Suckling, C. J. An evaluation of minor groove binders as anti-fungal and anti-mycobacterial therapeutics. *Eur. J. Med. Chem.* **2017***, 136*, 561-572.

46. Suckling, C. J.; Scott, F. Selectivity in anti-infective minor groove binders, *Proceedings of the 3rd International Electronic Conference on Medicinal Chemistry*, November 1, 2017. https://sciforum.net/paper/view/conference/4648

47. De Koning, H. P. Drug resistance in protozoan parasites. *Emerging Topics in Life Sciences.* **2017**, *1*, 627-632.

48. Wilkes, J. M.; Mulugeta, W.; Wells, C.; Peregrine, A. S. Modulation of mitochondrial electrical potential: a candidate mechanism for drug resistance in African trypanosomes. *Biochem J.* **1997**, *326*, 755-761.

49. Cerofolini, L.; Amato, J.; Borsi, V.; Pagano, B.; Randazzo, A.; Fragai, M. Probing the interaction of distamycin A with S100beta: the "unexpected" ability of S100beta to bind to DNA-binding ligands. *J. Molecular recognition.* **2015**, *28*, 376-384.

50. Vickerman, K. The fine structure of *Trypanosoma congolense* in its bloodstream phase. *J. Protozool*. **1969**, *16*, 54-69.

51. Frevert, U.; Reinwald, E. Endocytosis and intracellular occurrence of the variant surface glycoprotein in *Trypanosoma congolense*. *J. Ultrastruct. Mol. Struct. Res.* **1988**, *99*, 137-149.

52. Zoltner, M.; Horn, D.; De Koning, H. P.; Field, M.C. Exploiting the Achilles' heel of membrane trafficking in trypanosomes. *Curr Opin Microbiol.* **2016**, *34*, 97-103.

53. Castillo-Acosta, V. M.; Estévez, A. M.; Vidal, A. E.; Ruiz-Perez, L. M.; González-Pacanowska, D. Depletion of dimeric all-alpha dUTPase induces DNA strand breaks and impairs cell cycle progression in Trypanosoma brucei. *Int J Biochem Cell Biol.* **2008***, 40*, 2901-2913.

54. Coustou, V.; Guegan, F.; Plazolles, N.; Baltz, T. Complete in vitro life cycle of *Trypanosoma congolense*: development of genetic tools. *PLoS Negl Trop Dis.* **2010**, *4*, e618.

55. Räz, B.; Iten, M.; Grether-Bühler, Y.; Kaminsky, R.; Brun, R. The Alamar Blue assay to determine drug sensitivity of African trypanosomes (*T. b. rhodesiense* and *T. b. gambiense*) *in vitro*. *Acta Trop.* **1997**, *68*, 139-147.

56. Brun, R.; Kunz, C. *In vitro* drug sensitivity test for *Trypanosoma brucei* subgroup bloodstream trypomastigotes. *Acta Trop*. **1989**, *46*, 361-368.

57. Kaminsky, R.; Mamman, M.; Chuma, F.; Zweygarth, E. Time-dose-response of *Trypanosoma brucei brucei* to diminazene aceturate (Berenil) and in vitro simulation of drug-concentration-time profiles in cattle plasma. *Acta Trop.* **1993,** *54*, 19-30.

58. Mwenechanya, R.; Kovářová, J.; Dickens, N. J.; Mudaliar, M.; Herzyk, P.; Vincent, I.M.; Weidt, S. K.; Burgess, K. E.; Burchmore, R. J. S.; Pountain, A. W.; Smith, T. K.; Creek, D. J.; Kim, D. H.; Lepesheva, G. I.; Barrett, M. P. Sterol 14α-demethylase mutation leads to amphotericin B resistance in *Leishmania mexicana*. *PLoS Negl Trop Dis*. **2017**, *11*, e0005649.

59. Creek, D. J.; Jankevics, A.; Burgess, K. E.; Breitling, R.; Barrett, M. P. IDEOM: an Excel interface for analysis of LC-MS-based metabolomics data. Bioinformatics. **2012**, *28*, 1048-1049.

60. Gloaguen, Y.; Morton, F.; Daly R.; Gurden, R.; Rogers, S.; Wandy, J.; Wilson, D.; Barrett, M.; Burgess, K. PiMP my metabolome: an integrated, web-based tool for LC-MS metabolomics data. *Bioinformatics*. **2017**, *33*, 4007-4009.

61 Khalaf, A. I.; Pitt, A. R.; Scobie, M.; Suckling, C. J.; Urwin, J.; Waigh, R. D.; Fishleigh, R. V.; Young, S. C.; Wylie, W. A. The synthesis of some head to head linked DNA minor groove binders. *Tetrahedron*. **2000**, *56*, 5225-5239.

62. Ong, C. W.; Yang, Y-T.; Liu, M-C.; Fox, K. R.; Liu, P. H.; Tung, H-W. Synthesis of directly linked diazine isosteres of pyrrole-polyamide that photochemically cleave DNA. *Org. Biomol. Chem.* **2012**, *10*, 1040-1046.

For Table of Contents Only